Master's Thesis

Computation Performance Improvement Method of a Photovoltaic Cell Model for Power Hardware-in-the-Loop Simulation Test Platform

Sang-Kyu Kwak

Department of Electrical Engineering

Graduate School of UNIST

2018

Computation Performance Improvement Method of a Photovoltaic Cell Model for Power Hardware-in-the-Loop Simulation Test Platform

Sang-Kyu Kwak

Department of Electrical Engineering

Graduate School of UNIST

Computation Performance Improvement Method of a Photovoltaic Cell Model for Power Hardware-in-the-Loop Simulation Test Platform

A thesis/dissertation
submitted to the Graduate School of UNIST
in partial fulfillment of the
requirements for the degree of
Master of Science

Sang-Kyu Kwak

12. 15. 2017
Approved by

Advisor
Jee-Hoon Jung

Computation Performance Improvement Method of a Photovoltaic Cell Model for Power Hardware-in-the-Loop Simulation Test Platform.

Sang-Kyu Kwak

This certifies that the thesis/dissertation of Sang-Kyu Kwak is approved.

12. 15. 2017

signature

Advisor: Jee-Hoon Jung

signature

Katherine Ann Kim

signature

Jun Moon

Abstract

In the prototype development process, the product functional testing could be expensive and time-consuming. In various industries such as aviation, automobiles, and electric power, Hardware-In-the-Loop Simulation (HILS) is used in the product development process. By using HILS, the system which is linked with the developed product is configured by simulation to provide a virtual operating environment. So, a variety of functions can be tested in an environment similar to the actual before the final product development stage. HILS performs simulation in real time to simulate the system same as actual operation. Various technical problems arise in this process, and a lot of research has been going on to solve the problem.

In this paper, computation methods are proposed to improve the real-time simulation performance of a photovoltaic (PV) cell model for power hardware-in-the-loop simulation (PHILS) applications. In PHILS, high computation performance is required because the simulator should complete the target model calculations in a real-time manner without overrun errors. One solution is to reduce the computation time of the target model. To solve nonlinear PV cell model equations, numerical methods used for solving the nonlinear equations can be used. However, these methods can be computationally intensive. In order to optimize performance for PHILS, performance of Newton-Raphson and Halley's numerical methods are compared and methods for choosing an initial value are proposed, which affect the computation time of the numerical iterations. Using the proposed initial value decision methods, the computation time can be drastically reduced. The target PV cell model, in which the computation time improvement method is applied, is verified in static and dynamic conditions to verify the accuracy of the model in the PHILS system.

In addition, two PHILS tests were conducted to show examples of HILS for development of PV system power converter. First test is Maximum Power Point Tracking (MPPT) function test and second is to output the voltage of Differential Power Processing (DPP) converter model. Also, the real-time simulation for large-scale PV system is described to show the computation speed in extended model.

Contents

List of Figures

List of Tables

List of Abbreviations

CHILS	Control Hardware-in-the-Loop Simulation
DPP	Differential Power Processing
HILS	Hardware-in-the-Loop Simulation
HUT	Hardware Under Test
MPP	Maximum Power Point
MPPT	Maximum Power Point Tracking
MRE	Mean Relative Error
P&O	Perturb and Observe
PHILS	Power Hardware-in-the-Loop Simulation
PMS	Power Management System
PV	Photovoltaic
RTS	Real-Time Simulator
SC	Subsystem Console
SM	Subsystem Master
SS	Subsystem Slave

Ⅰ. Introduction

Photovoltaic (PV) power is a universal renewable energy source that has been widely used and developed to replace fossil fuels to preserve the global environment. With the development of photovoltaic systems, the entire system has become more complex, including power converters, cooling solutions and other system components. When developing a PV plant, the prototyping process should perform functional tests under various functional conditions. However, the development of the PV system depends on the environmental conditions and the irradiance, so the functional test can be delayed by the weather schedule and therefore a long time is required. In addition, power converters in PV systems should be tested under abnormal and fault conditions as well as normal conditions. Therefore, these functional tests are costly and time consuming in the development process.

Many industries use a test platform called HILS to solve this problem. HILS simulates a system which works with the Hardware-Under-Test (HUT). Fig. 1 shows Hardware-in-the-loop Simulation (HILS) concept. There are two kinds of HILS platform in power hardware: Control HILS (CHILS) and Power HILS (PHILS) shown in Fig. 1. CHILS is used to test a controller and PHILS is for a power hardware. Fig. 1 (a) shows concept of CHILS, the Real-Time Simulator (RTS) simulates a system and it acts like actual system. The controller can operate without the real system. In PHILS, additional device is used for power interfacing between the RTS and the HUT because the RTS cannot supply real power shown in Fig. 1 (b). In a PV system, CHILS can be used for a controller test of a power converter and PHILS can be used for function test of the power converter connected to the PV cell. In the PV PHILS system used in this paper, the RTS calculates a PV cell model, and emulates the its electrical operation. The power interface receives the voltage signal of the PV cell model sent from the RTS through the external input port and converts the voltage signal into the actual voltage to supply power. Using this PHILS platform, the power converter can be efficiently tested in the development process. In a real PV system, the power converter is connected to a real PV panel. However, in the PHILS system, the power converter receives power from the power interface controlled by the RTS. PV PHILS allows testing of large-scale PV systems by making the test cost-effective and time-efficient. It can also help to quickly prototype other equipment connected to the PV plant [1], [2].

PHILS requires RTS because it computes complex models in real time. Due to the performance limitations of RTS, previous studies have been performed to optimize simulation performance by reducing computation time [3]-[5]. The PV cell model uses the numerical solution to calculate the output voltage such as Newton-Raphson method and Halley's method [6]. Therefore, quick calculation of numerical solutions is an important performance criterion that can reduce model calculation time.

In previous research, several numerical methods and fast computation methods were proposed to

reduce the model computation time [3], [4]. An approach using an effective initial value is proposed for fast computation of numerical iteration [5]. This method can have a significant impact on model calculation time. The contents are described in the next section. The above-mentioned studies use an existing PV cell model which is called five-parameter model. This model has been used in many studies to observe PV cell characteristics [7], [8]. However, the five-parameter model does not accurately simulate reverse bias characteristics and thus exhibits limited dynamic characteristics. In actual PV system operation, various abnormal behaviors occur under reverse-biased conditions [9]. Therefore, in order to test the operation of the PV system, the PV cell should be modeled to simulate reverse-biased conditions.

In this paper, the PV cell model has reverse bias characteristics and it is combined with a thermal model for high accuracy of the PV cell model [10], [11]. With the electric-thermal PV cell model, the PV PHILS test can be performed using a PV cell model with improved calculation speed and accuracy. By comparing numerical solutions and using effective initial value estimation, the calculation speed is improved. To verify the computational speed of each numerical solution, Newton-Raphson and Halley's methods are applied to the PV cell model and the results are compared. The convergence speed of each numerical solution is analyzed according to the PV cell operating point. In addition, the effective initial value is estimated according to the operating conditions and applied to the numerical solution method, contributing to the calculation speed improvement.

The PV cell model to which the proposed method is applied is verified in two modes: static and dynamic situations. The static characteristics of the PV model are verified by off-line simulation, and the results are compared with the actual 1.3W PV cell experiments. The dynamic characteristics are verified using the PV PHILS system due to the delay of each device such as simulator and programmable power supply. In order to show the computation speed improvement in large scale model, the PV panel model simulation is described. After that, the simple example using PV PHILS system is described. The Maximum Power Point Tracking operation of the power converter is verified, and the power emulation of Differential Power Processing converter is shown.

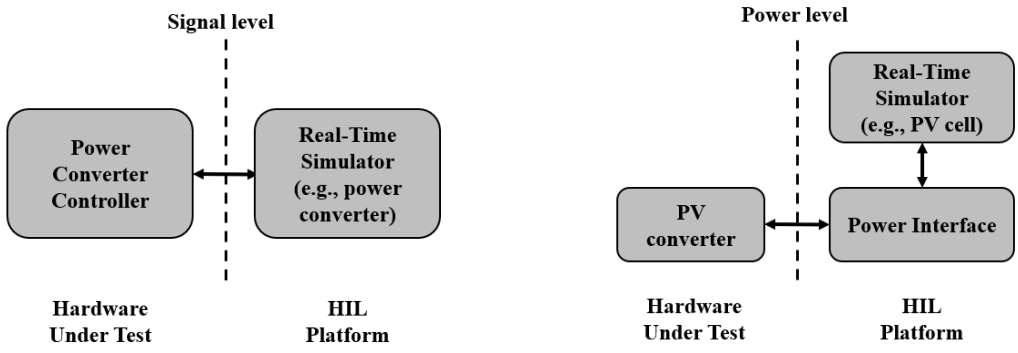

Fig. 1 Concept of HILS system: (a) Control HILS, (b) Power HILS

Ⅱ. Photovoltaic Cell Model

The PV cell model used in this paper is an electric-thermal PV cell model, which is divided into an electric model and a thermal model. The electric model simulates the electrical characteristics of the PV cell. The PV cell is represented by an electrical equivalent circuit, and the output voltage of the PV cell is obtained from the equivalent circuit. The thermal model is used to take into account that the electrical properties of the PV cell are affected by temperature. The temperature of the PV cell is obtained from the thermal model, and the value of this temperature is used to obtain the PV cell output voltage in the electric model. For the electric model, dynamic PV cell model is used to accurately simulate a PV cell in various operation conditions. With the dynamic PV cell model, the PV cell can be simulated both in forward and reverse biased region. Also, the dynamic model includes capacitive and inductive characteristics of a PV cell.

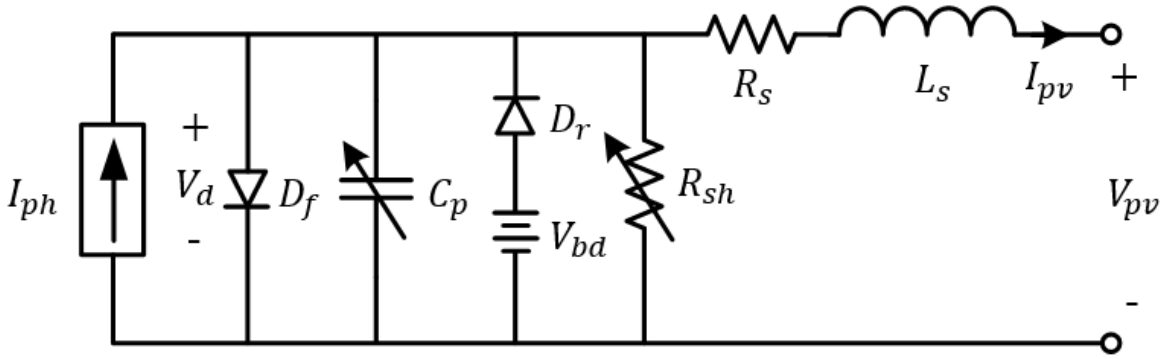

Fig. 2 Equivalent circuit of PV cell

2.1 Dynamic electric model

The output of the PV model is the output voltage V_{pv} shown in Fig. 2. The output voltage is determined from I_{pv} and V_d in (1).

$$V_{pv}\left(V_d, I_{pv}\right) = V_d - I_{pv}R_s - L_s\frac{dI_{pv}}{dt} \tag{1}$$

$$0 = I_{ph}\left(G,T\right) - I_{df}\left(T,V_d\right) - I_{Cp}\left(V_d\right) + I_{dr}\left(T,V_d\right) - I_{Rsh}\left(G,V_d\right) - I_{pv} \tag{2}$$

I_{pv} is output current but it is input value of the PV cell model. The power converter, which is connected to PV cell output, controls the PV cell's output current so it can be easily obtained. The V_d is voltage of forward diode. The value is obtained from Kirchhoff's Current Law. The current equation is nonlinear equation in (2) so it is solved with numerical method. The equation consists of

the current flowing through each component of the PV cell. The current equations are as follows

$$I_{ph}(G,T)=\left[I_{scn}\left(\frac{R_s+R_{sh}}{R_{sh}}\right)+K_i\left(T-T_n\right)\right]\frac{G}{G_n}\frac{M}{M_n} \tag{3}$$

$$I_{df}(T,V_d)=I_s\left[\exp\left(\frac{V_d}{aV_t(T)}\right)-1\right] \tag{4}$$

$$I_{dr}(T,V_d)=I_{sr}\exp\left(\frac{K_rV_{bd}}{aV_t(T)}\right)\left[\exp\left(\frac{-K_rV_d}{aV_t(T)}\right)-1\right] \tag{5}$$

Where I_{ph} represents the current of electrons excited by solar irradiance (3). The variables of this equation are irradiance G and PV cell temperature T. I_{scn} is nominal short-circuit current, R_s is series resistance, R_{sh} is shunt resistance and K_i is the current temperature coefficient, T_n is nominal temperature, G_n is the nominal irradiance, M is air mass in an area and M_n is nominal air mass. I_{df} is forward diode current that flows in the forward biased region. a is the diode ideality factor and I_s is diode saturation current. I_{dr} is reverse diode current where V_{bd} is breakdown offset voltage which it is negative value. I_{sr} is the reverse saturation current and K_r is the reverse breakdown scalar coefficient. The value of parallel capacitance C_p and shunt resistance R_{sh} is not constant. Their values are affected by an operating point, so the currents are also varied according to the operating point as follows

$$I_{Cp}(V_d)=C_p(T,V_d)\frac{dV_d}{dt} \tag{6}$$

$$C_p(T,V_d)=C_j(V_d)+C_d(T,V_d)+C_{bd}(V_d) \tag{7}$$

$$=\frac{C_{j0}}{\sqrt{1-\frac{V_d}{N_s\phi_0}}}+\frac{\tau I_{df}(T,V_d)}{aV_t(T)}+\frac{\tau_{bd}I_{dr}(T,V_d)}{aV_t(T)} \tag{8}$$

$$I_{Rsh}(G,V_d)=\frac{V_d}{R_{sh}(G)} \tag{9}$$

$$R_{sh}(G)=R_{shn}\frac{G_n}{G} \tag{10}$$

Where I_{Cp} is the parallel capacitor current. The parallel capacitor C_p consists of three different capacitances: junction capacitance C_j, diffusion capacitance C_d, breakdown capacitance C_{bd}. C_{j0} is zero-bias junction capacitance and ϕ_0 is zero-bias junction potential. τ is mean carrier lifetime. τ_{bd} is breakdown mean carrier lifetime. Equation (1)-(10) describes the step to obtain PV cell model output and they are described in detail in [10].

TABLE I PV CELL MODEL VARIABLES

Model Input	
G	Irradiance [W/m^2]
T	Temperature [$°C$]
I_{pv}	PV current [A]
Model Output	
V_{pv}	PV voltage [V]
Internal Parameters	
G_n	nominal irradiance [W/m^2]
T_n	nominal temperature [K]
Datasheet Parameters	
I_{scn}	nominal short circuit current [A]
V_{ocn}	nominal open circuit voltage [V]
I_{mpp}	maximum power point current [A]
V_{mpp}	maximum power point voltage [V]
K_i	current temperature coefficient [A/K]
Measured Parameters	
R_s	series resistance [Ω]
R_{shn}	nominal shunt resistance [Ω]
L_s	series inductance [H]
a	diode ideality factor
V_{bd}	breakdown voltage [V] (negative value)
I_{sr}	reverse saturation current [A]
K_r	reverse breakdown scalar coefficient
C_{j0}	zero-bias junction capacitance [F]
ϕ_0	zero-bias junction potential [V]
τ	mean carrier lifetime [s]
τ_{bd}	breakdown mean carrier lifetime [s]

The variables are listed in Table I. Some parameters can be obtained from Datasheet and the other parameters can be obtained through measurement in [10].

Fig. 3 Structure of PV cell

2.2 Thermal model

The temperature is a variable of the current equations. The temperature should be calculated accurately by applying thermal model. Since the calculation method of the temperature depends on the structure of the PV cell, the structure should be considered. The PV cell consists of 5 layers: layer 1 and 2 are glasses, layer 2, 4 are air layer and layer 3 is PV cell shown in Fig. 3. In the thermal model, an equation for a temperature change rate of a layer in (11) is used to calculate PV cell temperature by considering convection and radiation heat transfer of each layer in [11].

$$C_{lx}\frac{dT}{dt} = Q_{lw} + Q_{sw} + Q_{conv} + Q_{lx-y} - Q_{ele} \tag{11}$$

$$C_{lx} = A_{lx} \cdot d_{lx} \cdot p_{lx} \cdot C_{m-lx} \tag{12}$$

$$Q_{lx} = \sigma A_{l3}\left(\frac{1+\cos B}{2}e_s T_s^4 + \frac{1-\cos B}{2}e_g T_g^4 - e_p T^4\right) \tag{13}$$

$$Q_{sw} = a_{ab} \cdot G \cdot A_{l3} \tag{14}$$

$$Q_{conv} = -\left(h_{c,\,forced} + h_{c,\,free}\right) \cdot A_{lx} \cdot \left(T_{lx} - T_{amb}\right) \tag{15}$$

$$Q_{lx-y} = U_{ly} \cdot A_{ly}\left(T_{ly} - T_{lx}\right) \tag{16}$$

$$Q_{ele} = R_s I_{pv}^2 + \frac{\left(V_{pv} + R_s I_{pv}\right)^2}{R_{sh}} - V_{pv} I_{pv} \tag{17}$$

C_{lx} is the heat capacity of layer x where A_{lx} is area of layer x, d_{lx} is thickness of the layer, p_{lx} is density of material and C_{m_lx} is specific heat capacity of the material. Q_{lw} is a heat transfer from long wave radiation where σ is Stefan-Boltzmann constant, B is the tilted surface angle, e_s is the emissivity of the sky, T_s is effective sky temperature, e_g is the emissivity of the ground surface, T_g is the ground temperature and e_p is the emissivity of the PV cell. Q_{sw} is a heat transfer from short

wave radiation and a_{ab} is the absorbability of the PV cell surface. Q_{conv} is convection heat transfer where $h_{c,forced}$ is the forced convection coefficient, $h_{c,free}$ is the free convection coefficient, and $T_{ambient}$ is ambient temperature. Q_{lx-y} is heat transfer from layer y to x where U_{ly} is the heat transfer coefficient from layer y, A_{lx} is the area of layer x and T_{lx} is temperature of layer x. Q_{ele} is the heat transfer from electrical energy loss in the PV cell resistor. The electrical energy loss can be obtained from the electrical model of the PV cell. Using the equations (11) to (17), the temperature of each layer is obtained as follows

$$C_{l1}\frac{dT_{l1}}{dt} = Q_{conv1} + Q_{l1-2} \tag{18}$$

$$C_{l2}\frac{dT_{l3}}{dt} = Q_{l2-1} + Q_{l2-3} \tag{19}$$

$$C_{l3}\frac{dT_{l3}}{dt} = Q_{lw} + Q_{sw} + Q_{3x-2} + Q_{3x-4} - Q_{ele} \tag{20}$$

$$C_{l4}\frac{dT_{l4}}{dt} = Q_{l4-3} + Q_{l4-5} \tag{21}$$

$$C_{l5}\frac{dT_{l5}}{dt} = Q_{conv5} + Q_{l5-4} \tag{22}$$

Layer 1 and 5 are glass layers. They are between outside and air layers, so their heat transfer equations are affected by convection and conduction heat flow in (18) and (22). Layer 2 and 4 are top and bottom air layers. They are enclosed by glass and the PV cell layer, so heat transfer equations of the layers include only conduction heat flow in (19) and (21). PV cell absorbs sun light and generate electric power, so heat transfer equation of the PV cell layer includes long and short-wave radiation, conduction and heat from electric loss in (20). With the equation (18)-(22), the temperature of PV cell can be calculated, and it goes into the input of the electric model.

2.3 Model dynamics

As mentioned above, the dynamic PV cell model is used in this paper rather than the five-parameter PV cell model used in most of previous papers in [3]-[5]. Fig. 4 shows the equivalent circuit of the five-parameter PV cell model. This model does not include reverse diode and breakdown voltage, so it can only simulate the operation of a PV cell in the forward biased region. Fig. 5 shows the I-V curve of the actual PV cell, dynamic PV model, and the five-parameter model. In the forward region, the results of both models are very similar, but a difference can be easily seen in the reverse region. In a dynamic model, a reverse diode can conduct at a voltage lower than the breakdown voltage, so it

exhibits better accuracy under the region. For testing functions of a PV power converter, it should be operated in various PV cell operation points. Therefore, this dynamic PV cell model should be used for the PV PHILS system.

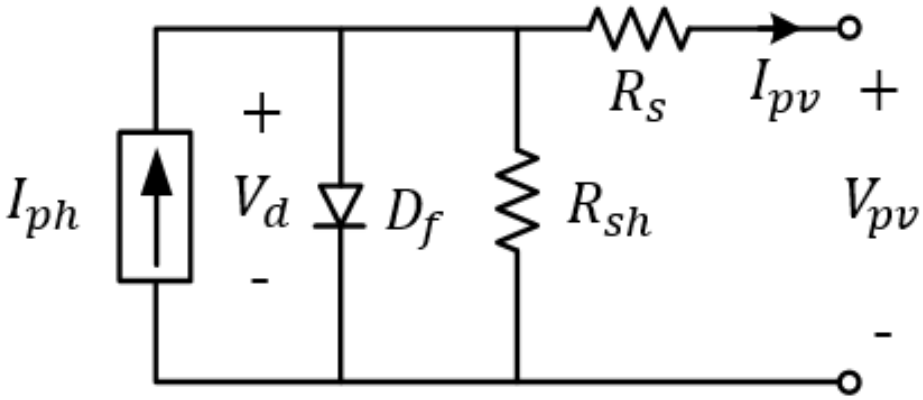

Fig. 4 Equivalent circuit of five-parameter model

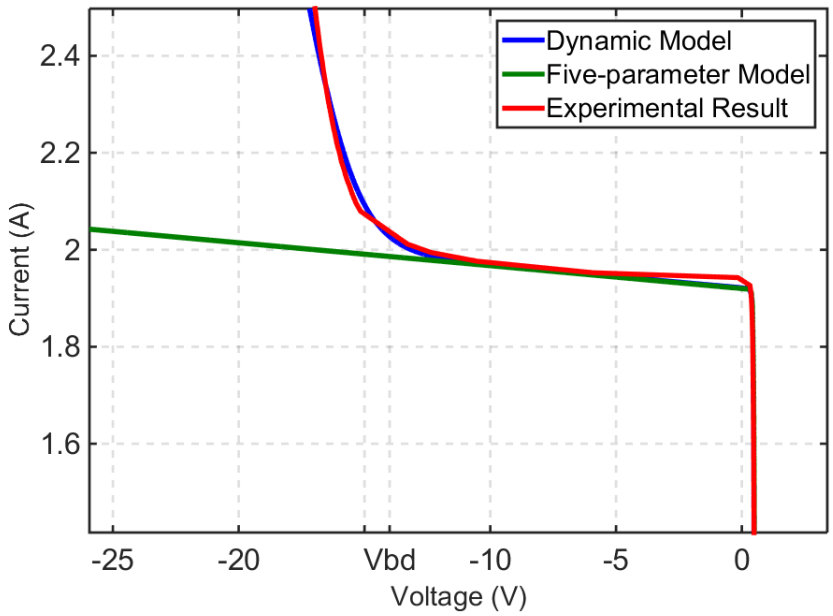

Fig. 5 Comparison of I-V curve among models and actual PV cell

Ⅲ. Real-Time Simulation Model and PHILS System

It is difficult to calculate model and output the results in real time because of limitation of performance with general PC. The real-time simulator can calculate the model in real time and output the calculated value to the external port. So, the real-time simulator in the HILS system configuration has a large role. In this paper, OPAL-RT OP5600 real-time simulator is used. The real-time simulator of OPAL-RT uses a simulation program based on MATLAB / SIMULINK. This real-time simulator works with a power interface device that receives signals and converts them to power. By connecting the simulated PV cell to the power converter, the PHILS test can be carried out.

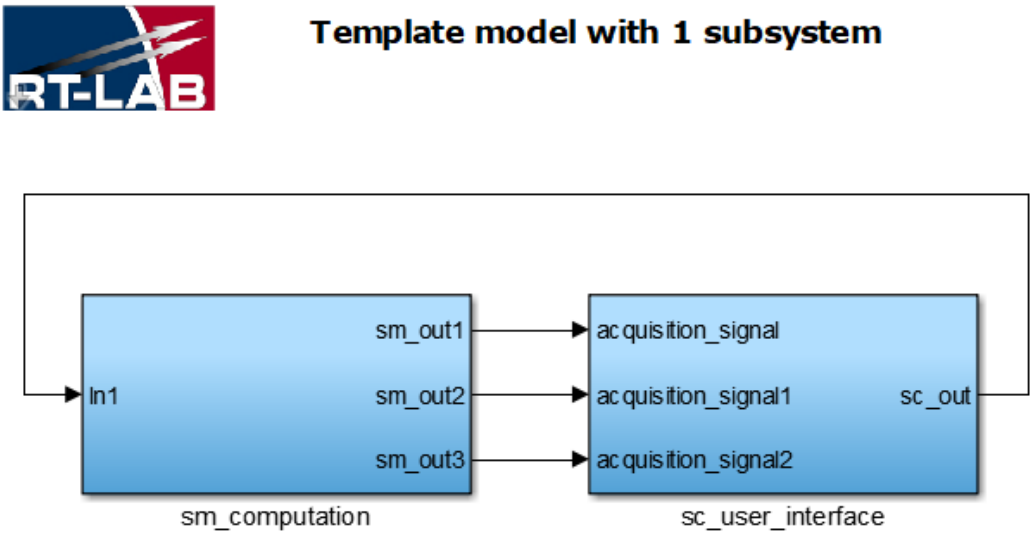

Fig. 6 Model Configuration for real-time simulation

3.1 Real-Time simulation model

In order to simulation a model with OPAL-RT Simulator, there are some rules such as model configuration and simulation time step. Fig. 6 shows basic model structure according to the rules. The entire model is divided into two subsystems: Subsystem Console (SC) and Subsystem Master (SM). SM includes PV cell model computed by the real-time simulator. SC is for the control of the model input parameters and monitoring of the model results and they are carried out in PC by user. During real-time simulation, the PC and real-time simulator communicates each other. The PC sends signals to real-time simulator about the PV system environment such as air mass and ambient temperature. From the input signals, the simulator computes the PV cell model and send the output result to PC so

that the output of PV cell models can be monitored in PC. In this way, a real-time simulation is performed.

One of the main functions of the OPAL-RT simulator is parallel computation. There are multiple cores in the simulator for parallel computing. In parallel computation, the model is divided into several subsystems and the systems are distributed to each core shown in Fig. 7. Thus, in parallel calculation, calculation time can be reduced because the model is computed by multiple cores rather than single core.

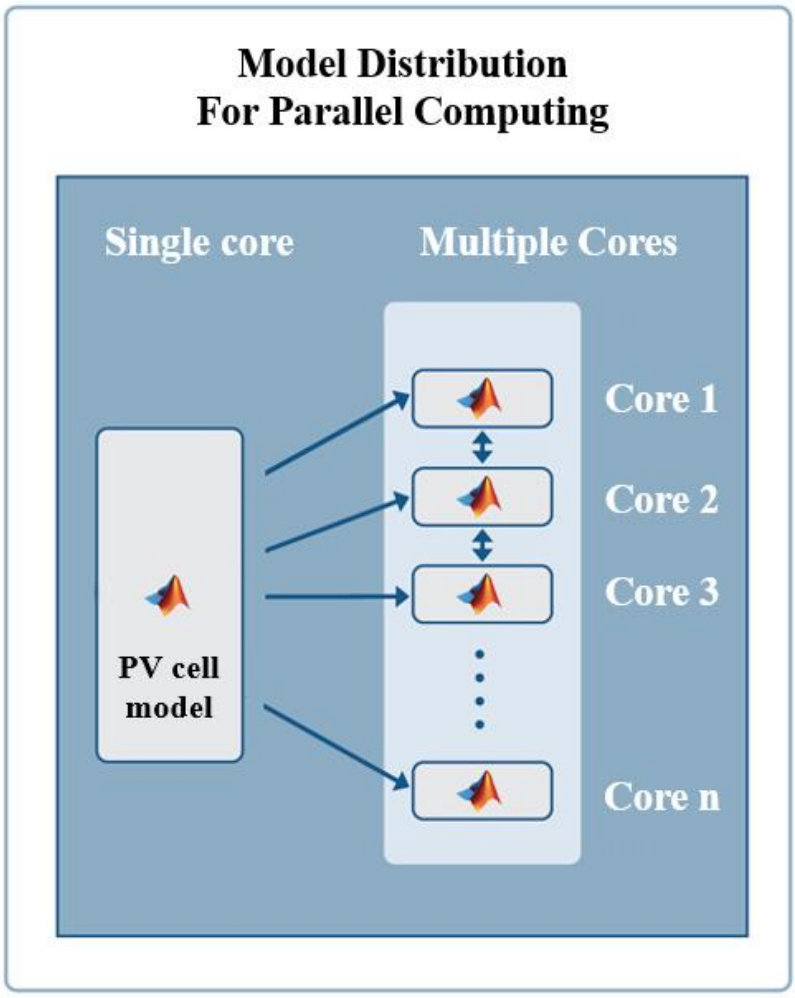

Fig. 7 Model separation for parallel computation

Fig. 8 (a) shows PV cell model configuration for parallel computation. As above mentioned, there are two models in PV cell model: electric and thermal model. In this paper, two cores are used, and each model is assigned to each core. SM has electric model of PV cell and Subsystem Slave (SS) has thermal model of PV cell. The models communicate each other because they are dependent each other as already explained in section II. The SC is not assigned to a core because this is for just monitoring

and parameter setting shown in Fig. 8 (b). Fig. 8 (c) shows the electric model and the equations in section 2.1 is programmed with MATLAB code in the PV cell model. Fig. 8 (d) shows thermal model and there are five models for each layer of PV cell. The temperature equations of each layer are also programmed in the model. It can be seen that the temperature models exchange their output results because the temperature of the layer is affected by adjacent layers. The Opcomm block must be used to get signal from other subsystem and the memory block should be used in parallel computation in [4]. They are rules for real-time simulation to use OPAL-RT simulator.

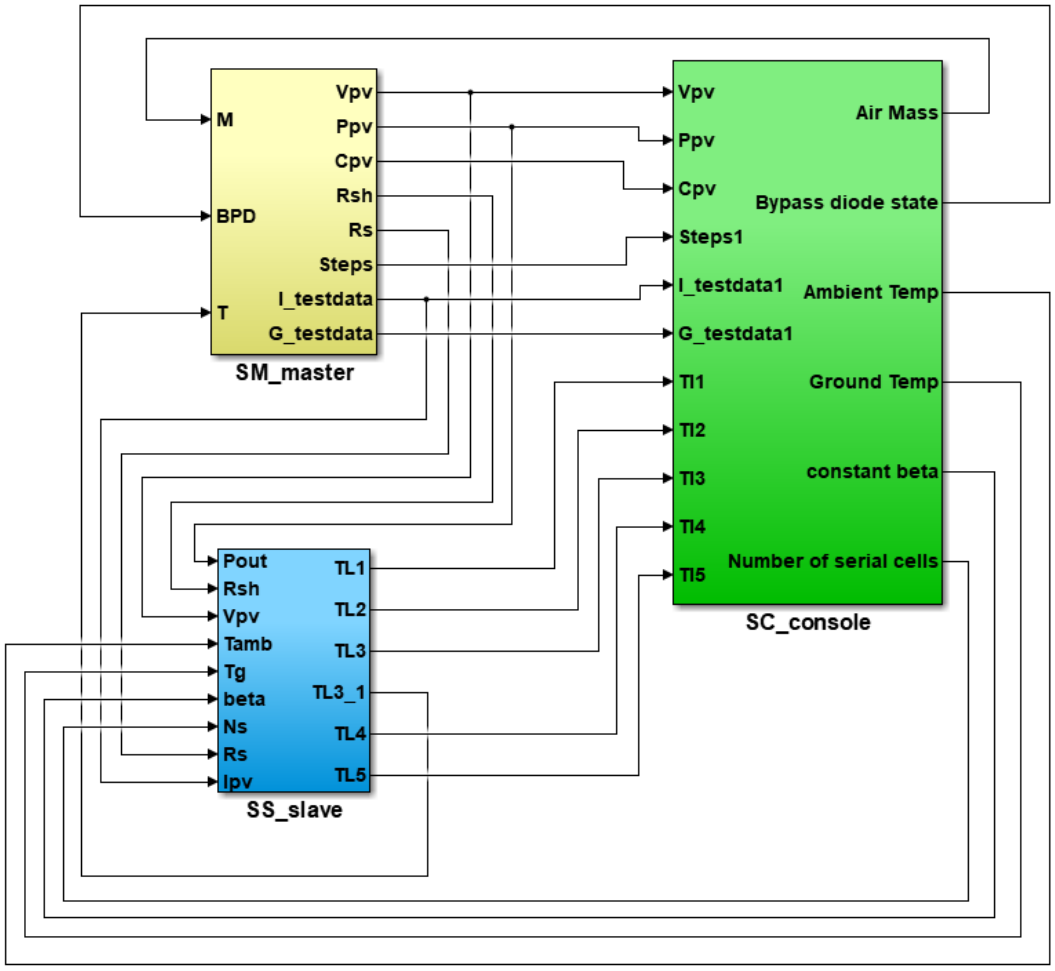

(a)

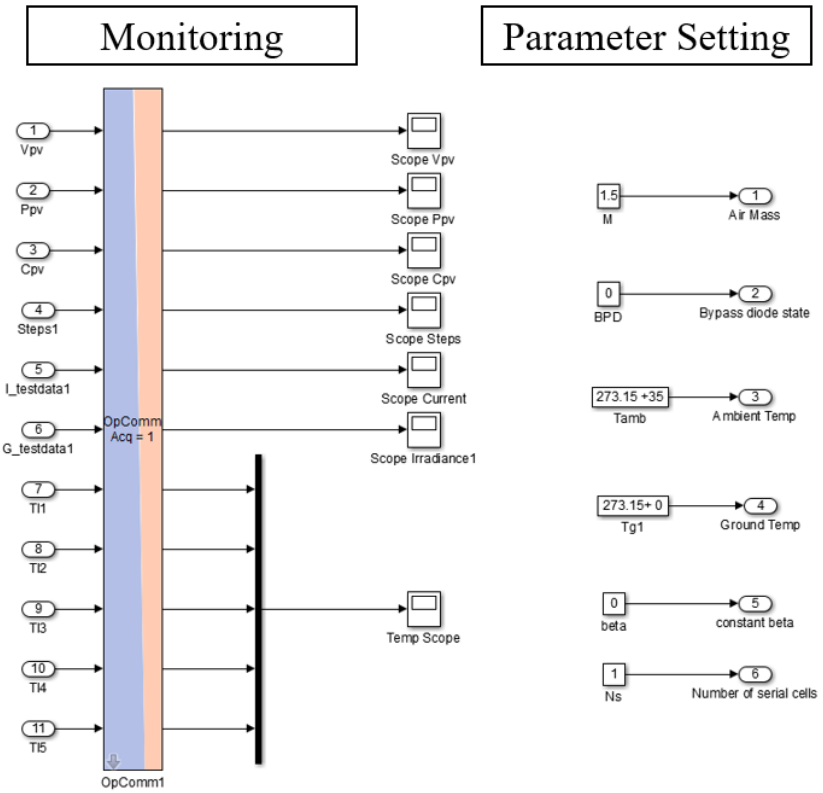

(b)

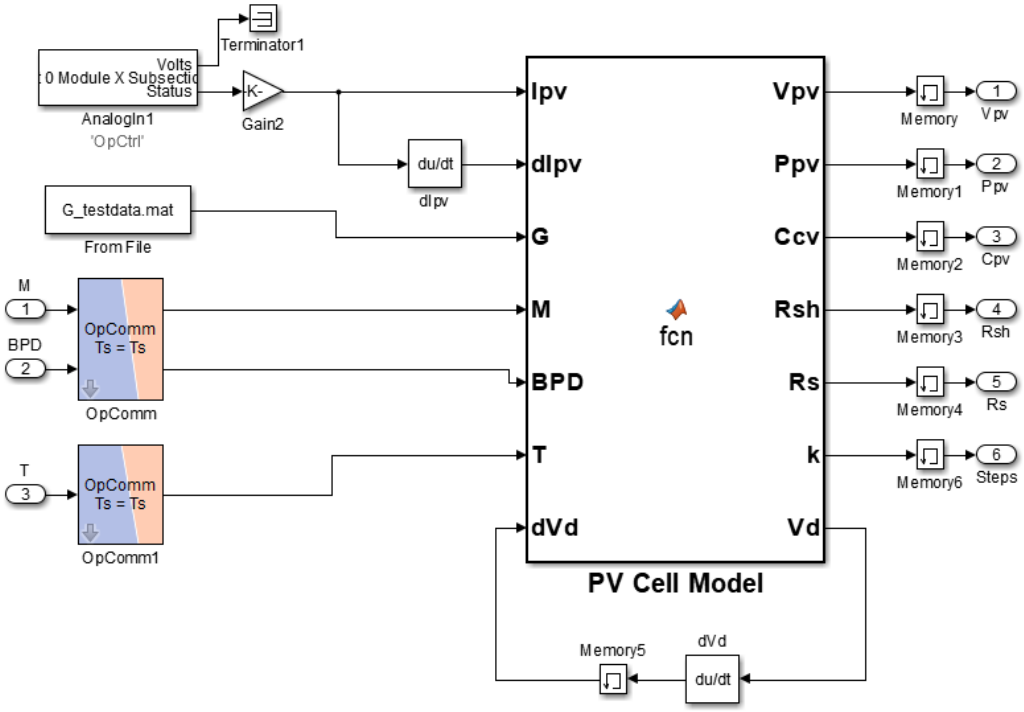

(c)

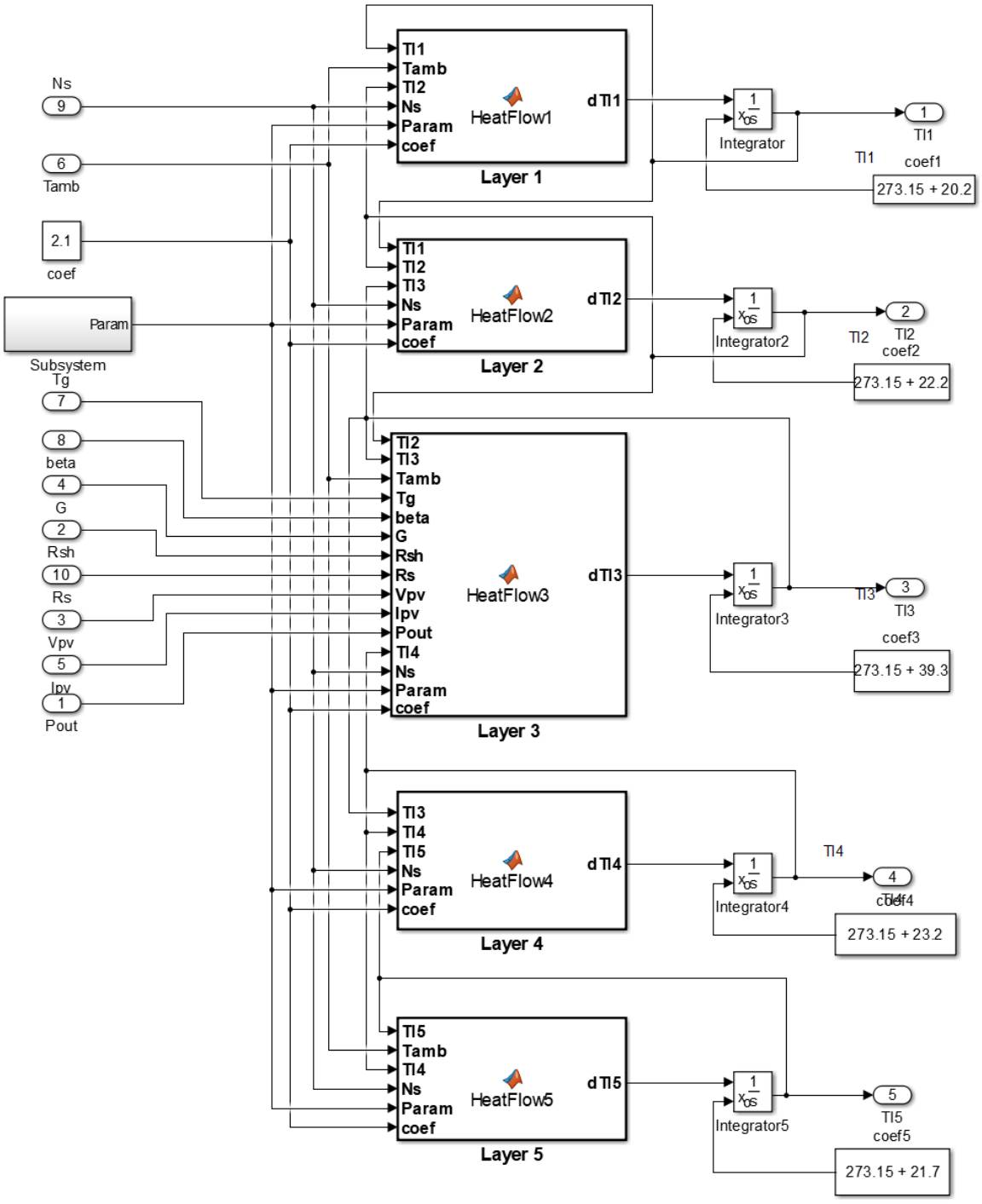

(d)

Fig. 8 PV Cell Model Configuration: (a) Integrated model for real-time simulation, (b) Monitoring and control, (c) Electrical model and (d) Thermal model

3.2 PHILS system

The PV cell operates with power converter shown in Fig. 9 (a). Power Converter controls current of PV cell to operate the PV cell in Maximum Power Point (MPP) condition. The PHILS system is used to test the function of the power converter in various PV cell operating points. Fig. 9 (b) shows the PHILS diagram which is set up in this paper. The PC, real-time simulator and programmable DC power supply simulates the same operation as real PV cell. The simulator computes the PV cell model and send the PV cell output voltage signal to the power supply and it converts the signal to real power, which is supplied to power converter. As mentioned in section 2, the PV cell's output current is input parameter of the PV model, so the power supply measures the current and feedback the value as signal to real-time simulator. This paper does not focus on development of power converter. Therefore, the real power converter is not used in the system. The source meter, which is controlled by python code, act as power converter and it can also operate the PV cell in MPP condition.

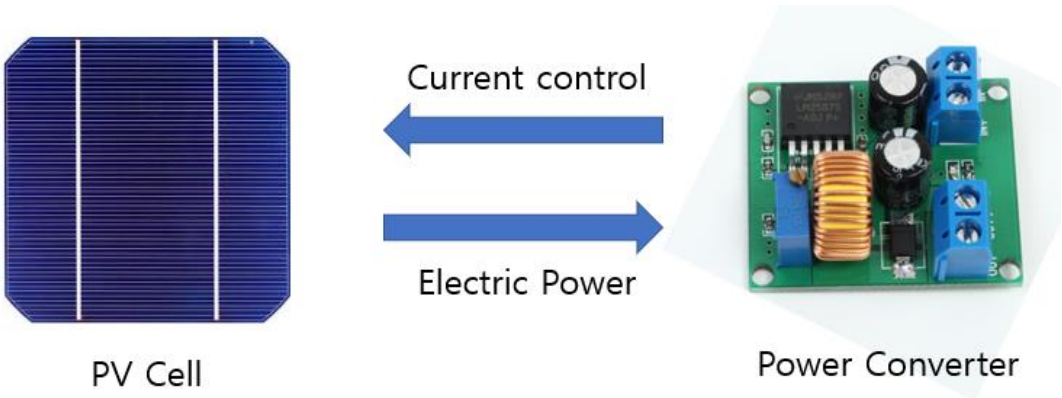

(a)

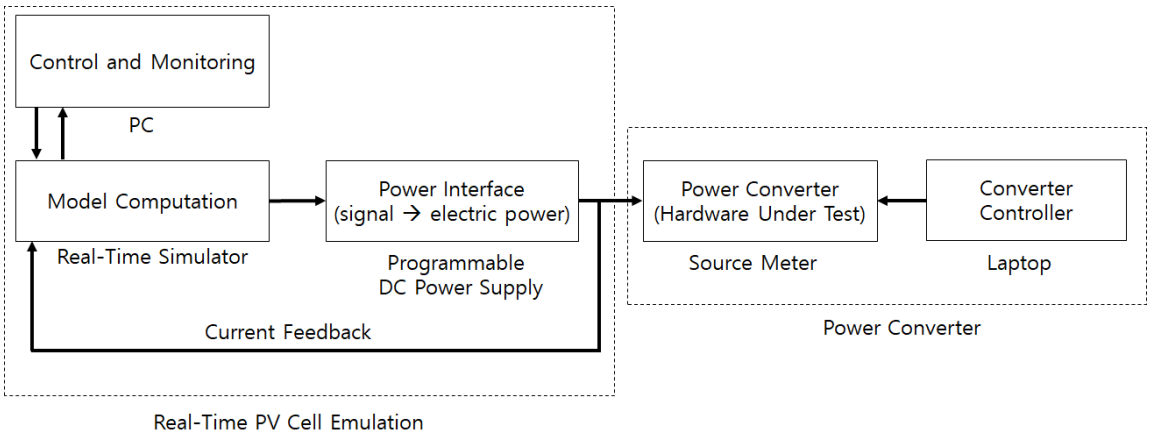

(b)

Fig. 9 PV cell connected to power converter (a) Real PV cell and power converter (b) Proposed PHILS diagram

Fig. 10 (a) shows the experimental setup of the PV system. A crystalline PV cell is used, and the rated power is 1.3 W. Peripheral equipment consists of a temperature sensor, an irradiation sensor, two multimeters and a source meter. The Kikusui DME1600 digital multimeters store measured values from an irradiation sensor and a temperature sensor. The Keithley 2430 source meter is connected to a PC and is operated by a program which is Maximum Power Point Tracking (MPPT) algorithm. Fig. 10 (b) shows the PV PHILS system setup. The difference from the experimental setup that the real PV cell is replaced with the simulation equipment and the PHILS system uses the stored irradiance data.

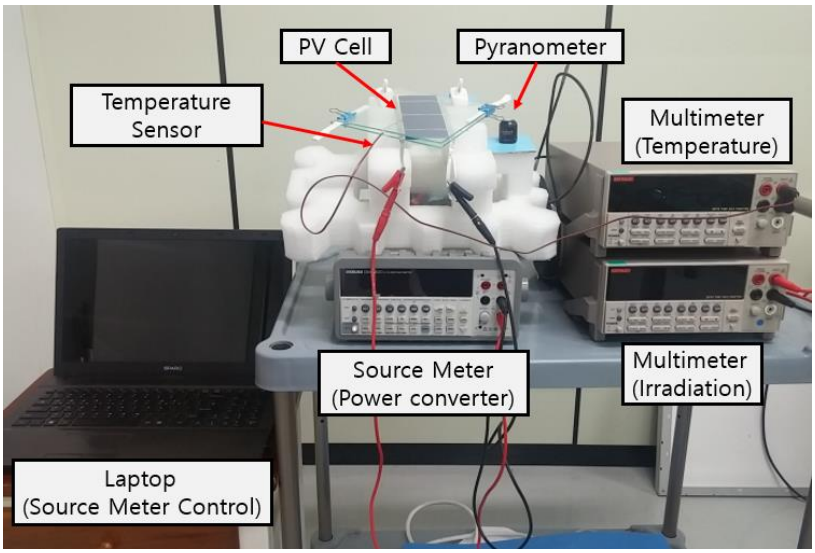

(a)

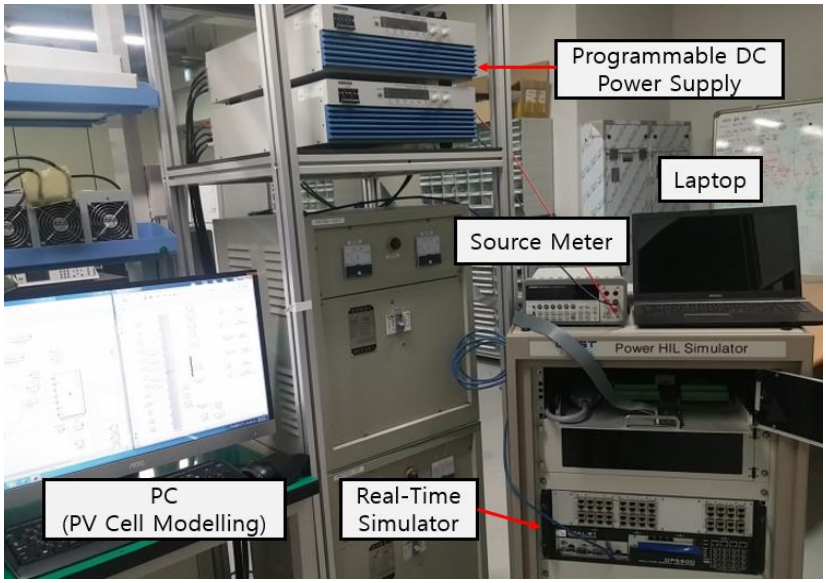

(b)

Fig. 10 PV system setup (a) Real PV system (b) PV PHILS system

IV. Optimization of Model Computation Time

The numerical solution is to find a value which is almost similar to the root of the function through the iterative method, rather than the exact value determined with the analytical method. There are various kinds of numerical solutions and convergence speeds are different according to each numerical solution. Therefore, the appropriate numerical method should be used by considering the characteristics of the function. In this paper, Newton-Raphson (NR) method and Halley's method, which are commonly used in PV cell model, are applied to PV cell model and their results are described. In addition, the initial value has a large effect on the calculation time of the numeric iterations. If the initial value is close to the final value of the numerical iteration, the calculation time would be short. The three initial value choice methods are described, and the methods are applied to the PV cell model. The results of each method are compared.

4.1 Numerical solutions for PV cell model

In the PV cell model, a numerical solution is used to find the value of V_d, the voltage of the forward diode and the equation (2) is applied to the numerical method. Newton-Raphson (NR) method in [13] are derived from the Taylor series as follows

$$f(x) = f(x_n) + f'(x_n)(x - x_n) + \frac{1}{2} f''(x_n)(x - x_n)^2 + \dots \tag{23}$$

$$f(x) \approx f(x_n) + f'(x_n)(x - x_n) \tag{24}$$

$$f(x) = 0 \tag{25}$$

$$x_{n+1} = x_n - \frac{f(x_n)}{f'(x_n)} \tag{26}$$

$$\Delta x = x_{n+1} - x_n = -\frac{f(x_n)}{f'(x_n)} \tag{27}$$

The NR method uses the approximated equation from the Taylor series and it finds the root x which makes the function $f(x)$ zero. Fig. 11 shows the concept of the NR method. The initial value x_1 is an arbitrary value set by the user and the NR method searches for root by iteration of the equation (26). x_n is the value obtained from the n^{th} iteration. Δx means the difference of the value in next step and current step. The value of Δx makes x_n approach to actual root by iterating the equation. If the function of $f(x)$ is almost equal to zero, the iteration stops and the final value of x is chosen as the root. The standard of stopping iteration is determined by a user.

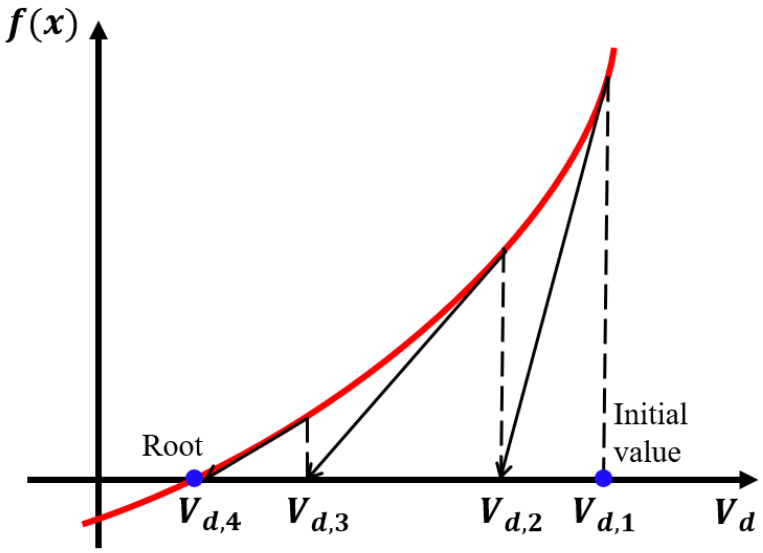

Fig. 11 Concept of Newton-Raphson method

Halley's method in [4] is also derived from the Taylor series as follows

$$f(x) \approx f(x_n) + f'(x_n)(x - x_n) + \frac{1}{2} f''(x_n)(x - x_n)^2 \tag{28}$$

$$0 = f(x_n) + f'(x_n)(x_{n+1} - x_n) + \frac{1}{2} f''(x_n)(x_{n+1} - x_n)^2 \tag{29}$$

$$0 = f(x_n) + (x_{n+1} - x_n)\left[f'(x_n) + \frac{1}{2} f''(x_n)(x_{n+1} - x_n) \right] \tag{30}$$

$$x_{n+1} = x_n - \frac{f(x_n)}{f'(x_n) + \frac{1}{2} f''(x_n)(x_{n+1} - x_n)} \tag{31}$$

$$x_{n+1} = x_n - \frac{2 f(x_n) f'(x_n)}{2\left[f'(x_n) \right]^2 - f(x_n) f''(x_n)} \tag{32}$$

The difference between the NR and Halley's method is that Halley's method includes the second derivative of the Taylor series. Therefore, Δx of Halley's method is different from that of the NR method. Fig. 12 shows the concept of Halley's method. It can be seen that the Halley's method has faster convergence speed than the NR method because the approximation is based on a hyperbola.

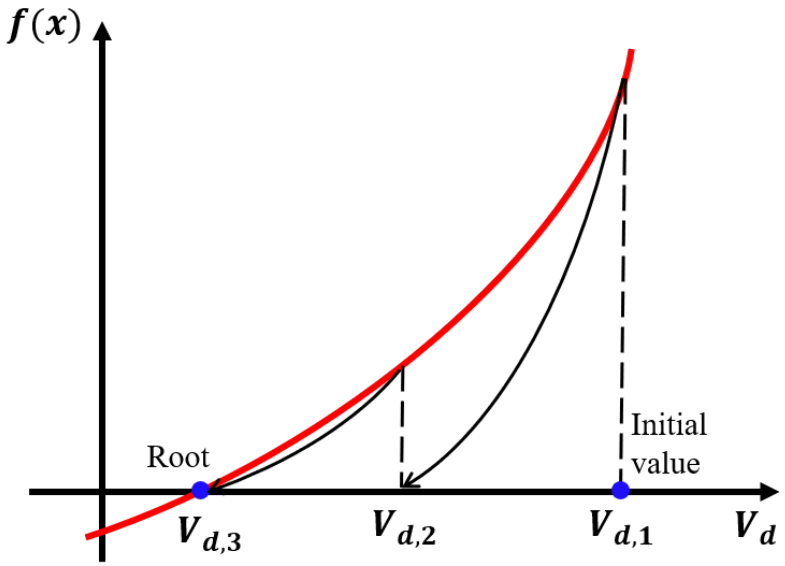

Fig. 12 Concept of Halley's method

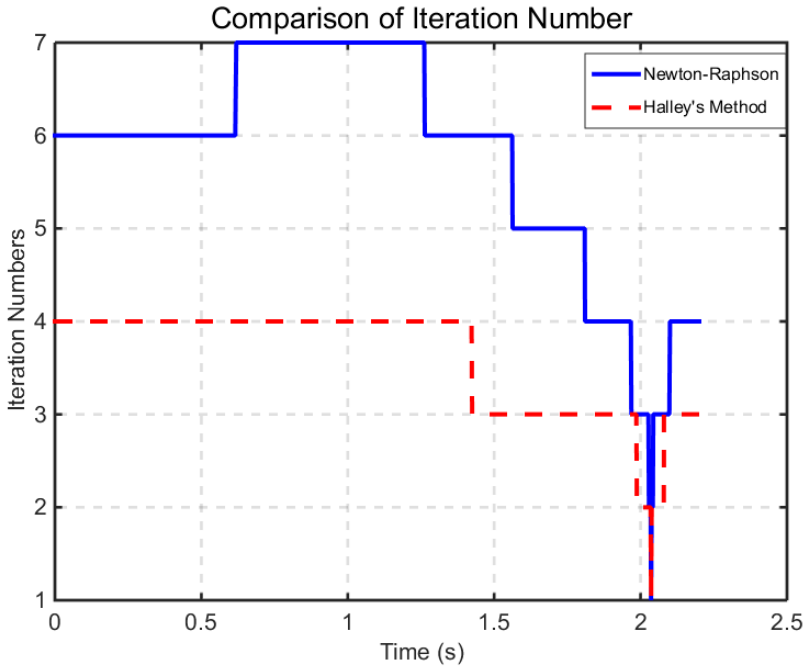

Fig. 13 Comparison of iteration number

Fig. 13 shows the iteration number of each method. The lower iteration number means fast computation. In most cases, the iteration number of Halley's method is lower than that of the NR method. The iteration numbers change according to PV cell operation point. The PV cell model operates in the forward biased region.

In the numerical solution, convergence should be considered. The numerical solution finds root

using approximated equation, so it does not always converge. The NR method does not have convergence criterion in [13]. The convergence depends on the accuracy of the initial value and the nature of the function. Therefore, in order to apply the numerical solution, the characteristics of the function must be analyzed to determine convergence. Fig. 14 shows four cases in which the NR method has poor converge. In that figure, the poor convergence cases can be easily seen. However, the determination of convergence is not always easy because it may not be found out by the shape of the function.

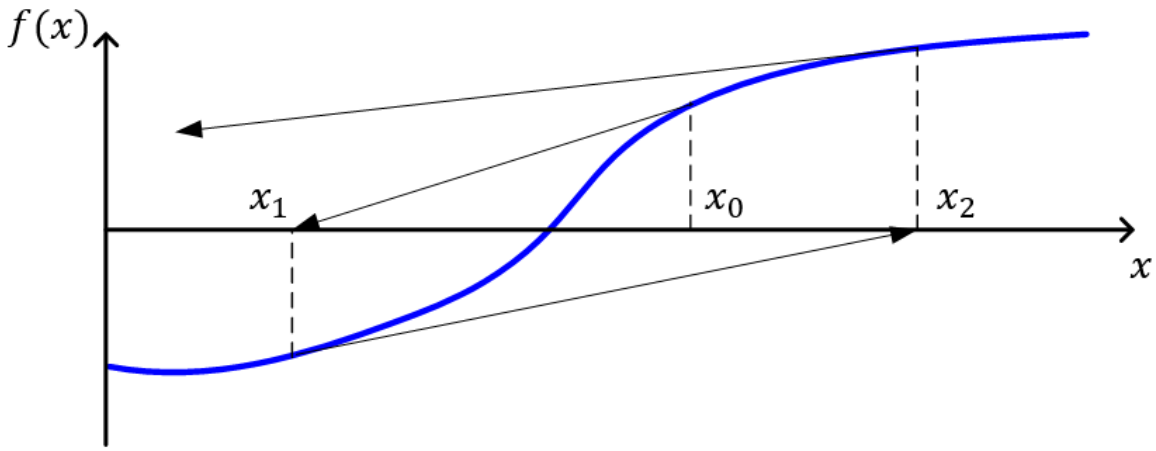

(a)

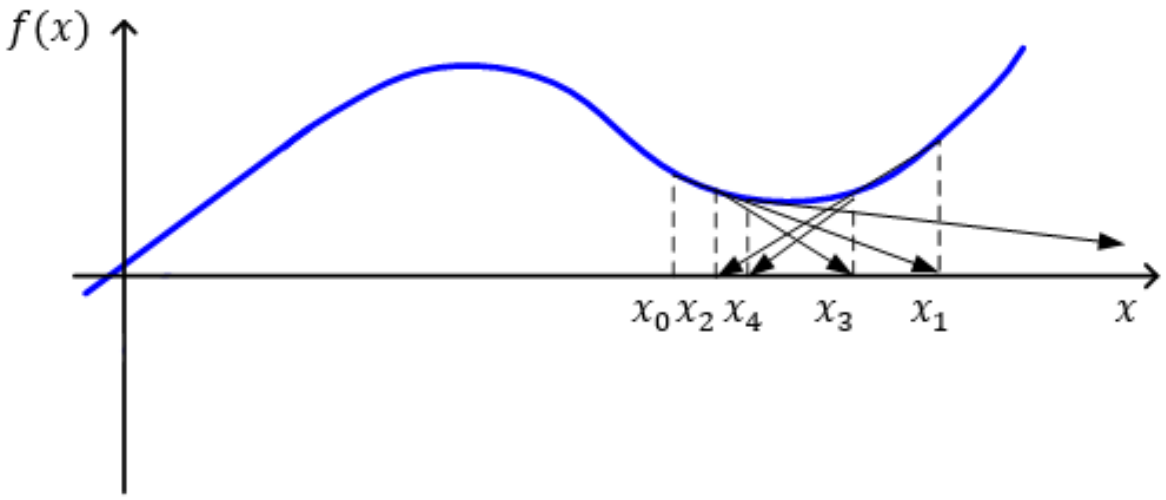

(b)

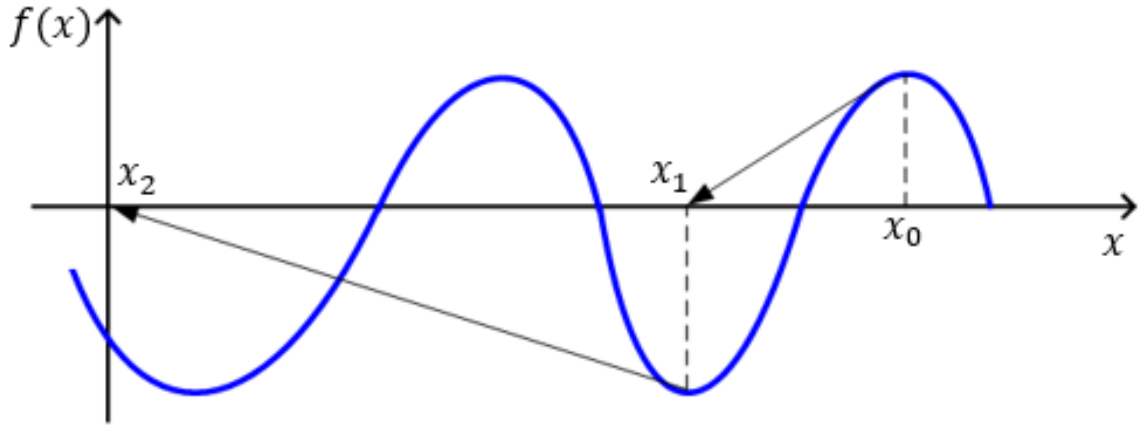

(c)

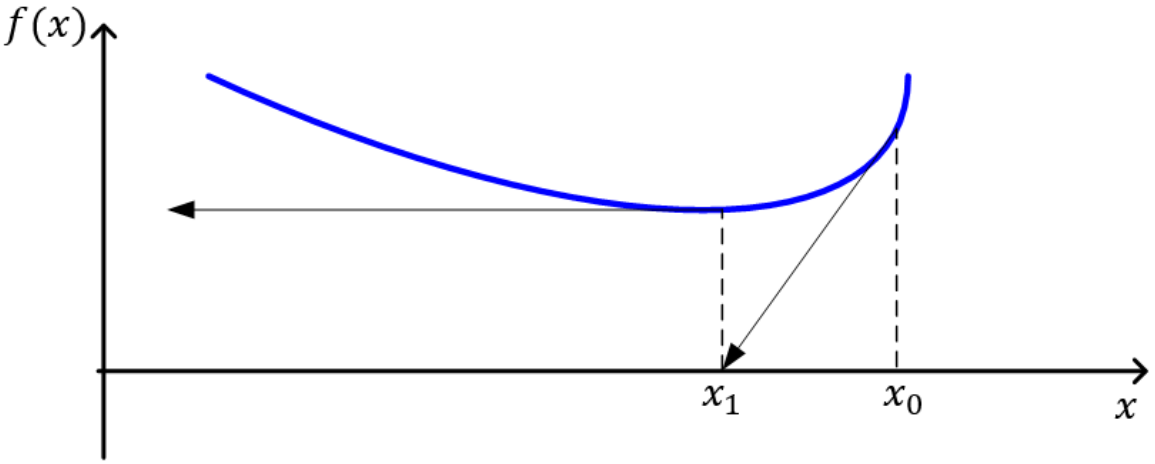

(d)

Fig. 14 Cases where the Newton-Raphson method has poor convergence: (a) First case, (b) Second case, (c) Third case, and (d) Forth case

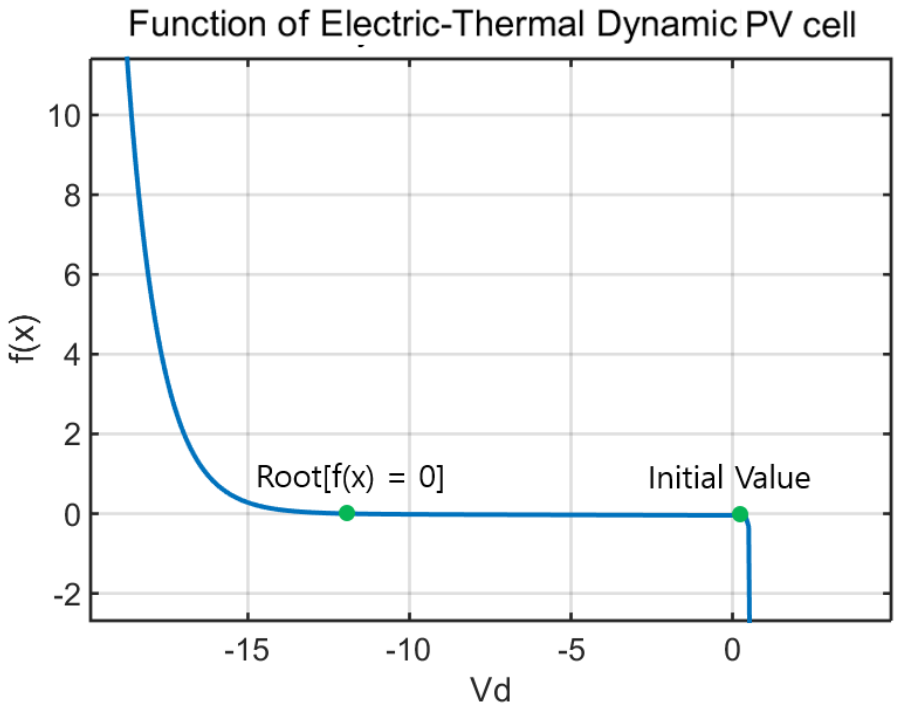

(a)

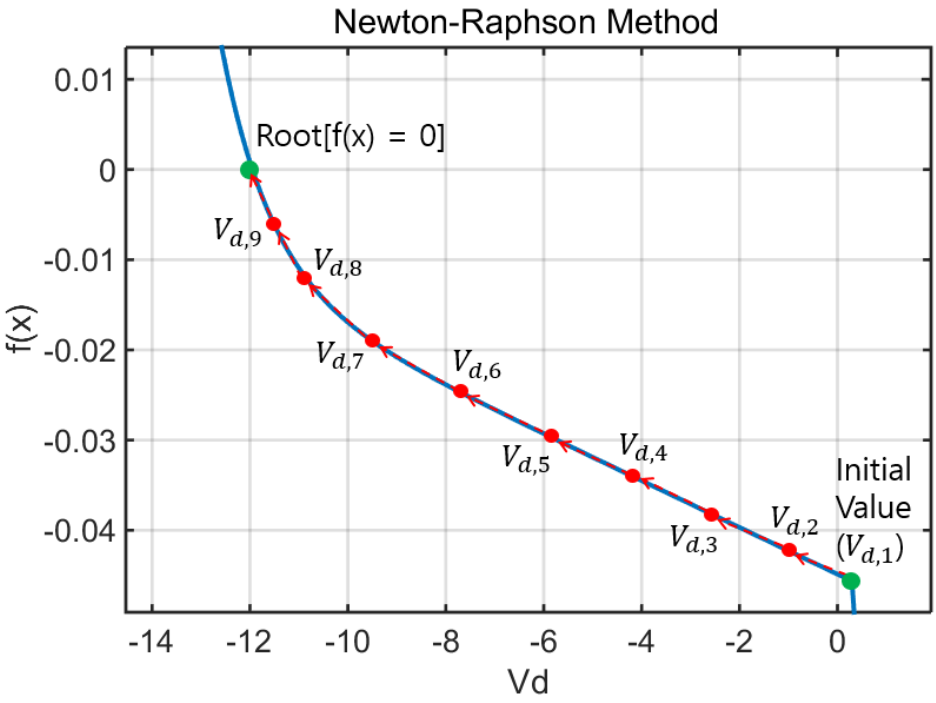

(b)

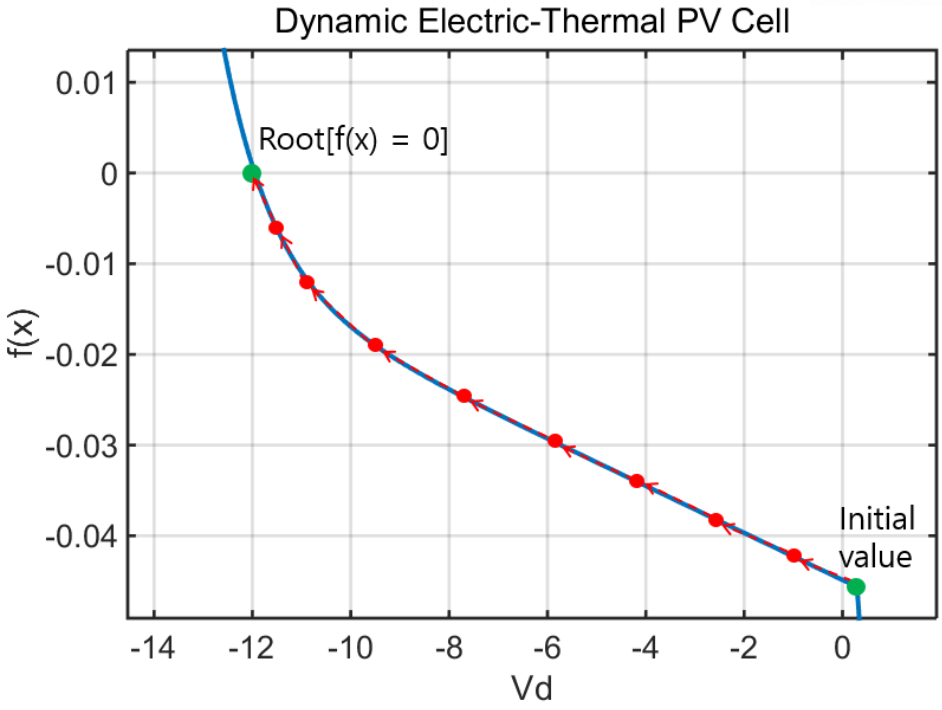

(c)

Fig. 15 Computation Process: (a) Original function of PV cell, (b) Newton-Raphson method, and (c) Halley's method

Fig. 15 (a) shows the function graph of the electric-thermal PV cell dynamic model according to V_d. For the model, the NR method converges over the entire region. Fig. 15 (b) shows the numerical computation using the NR method, which converges to the root. However, there are some conditions where the root of the model does not converge using Halley's method, which is shown in Fig. 15 (c). The exact root is -12 V, however, V_d at 0.11 V goes in the opposite direction of the actual root. In Halley's method, Δx in (27) is located at the second term of the right side of (32). The calculated value of Δx is 35.6, so the next value of V_d is 35.71 V. However, the maximum value of the Δx is limited to 0.55 so the next value of V_d becomes 0.66. From the point, it tries to go to the root, which is -12V, but it gets back to the initial value. Therefore, the iteration rotates in the infinite loop and Halley's method cannot converge in this condition.

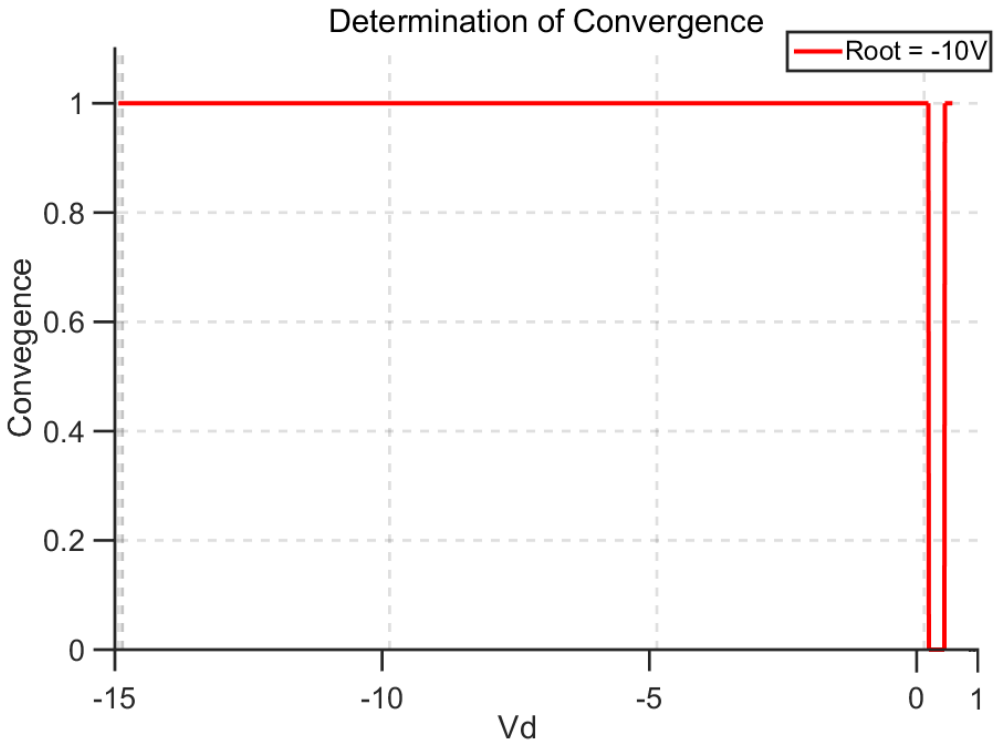

(a)

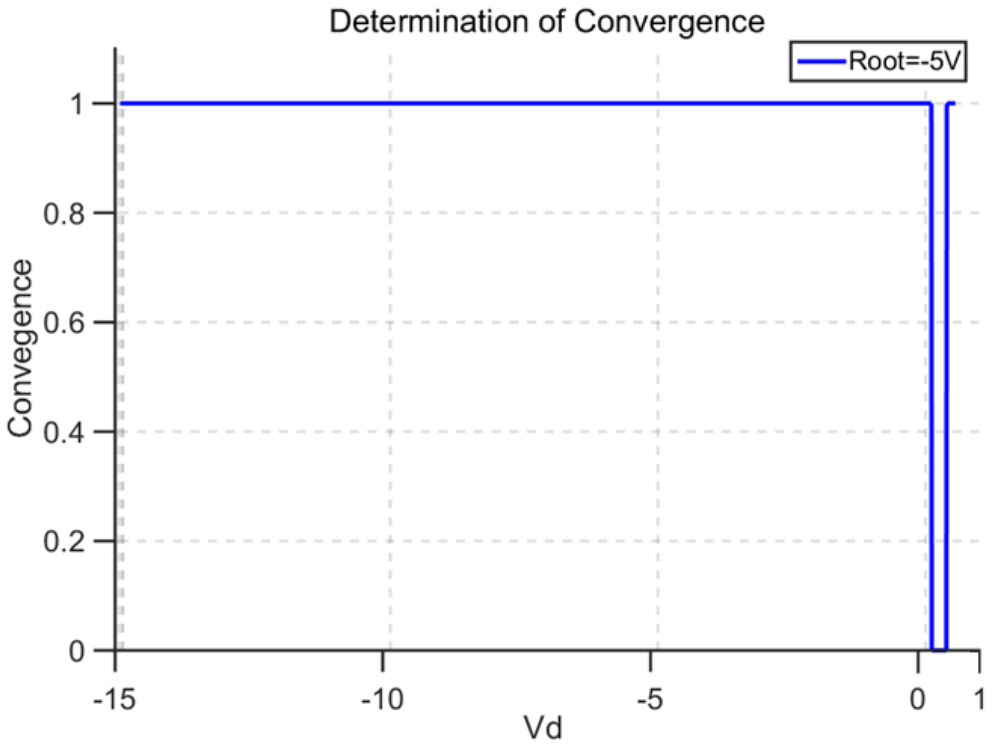

(b)

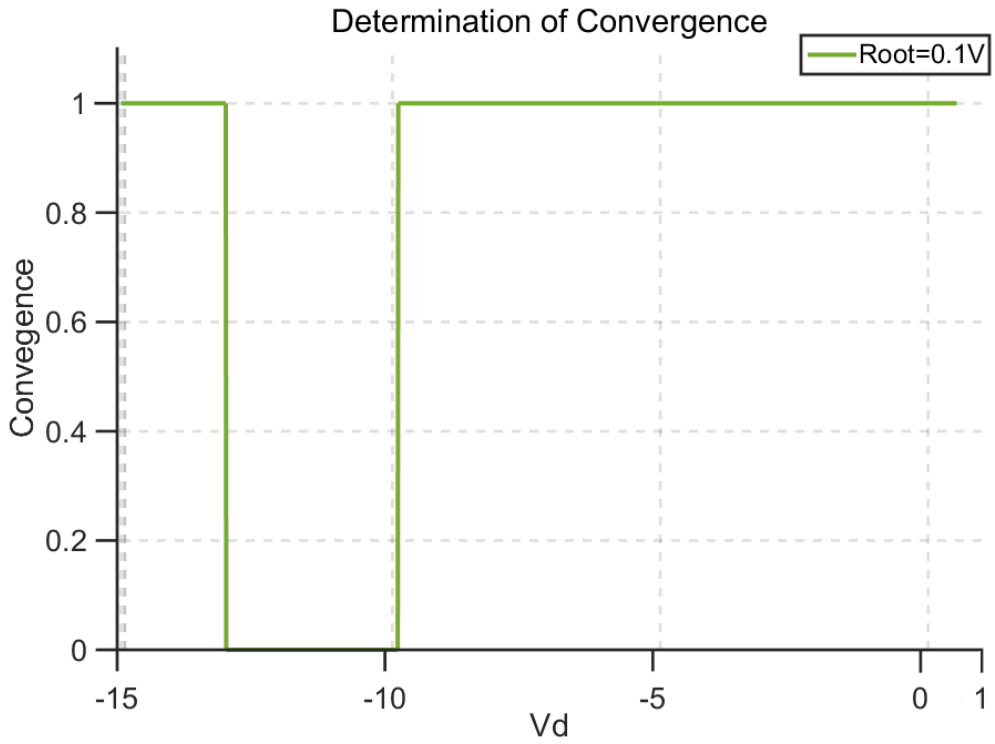

(c)

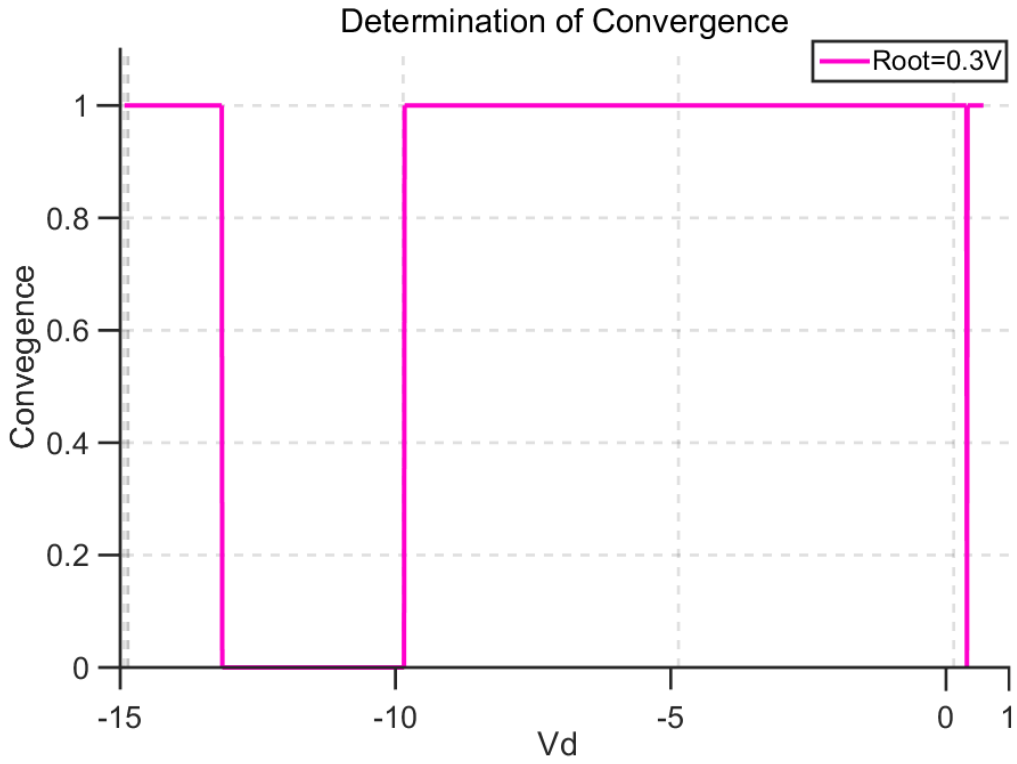

(d)

Fig. 16 Determination of convergence based on final value: (a) Final value = -10V, (b) Final value = -5V (c), Final value = 0.1V, and (d) Final value = 0.3V

The non-convergent cases can be observed by using MATLAB code. With the code, it can be found out where the $V_{d,n}$ goes to the opposite direction of the root. Fig. 16 shows the convergence and non-convergent cases. The PV cell model is operated in various conditions where the root of V_d is -10, -5, 0.1, 0.3. The root can be controlled by adjusting the input parameters of the PV cell model such as irradiance and temperature.

When the numerical solution is used for the value of V_d corresponding to the x-axis, the y-axis shows its convergence. If value of y-axis is "1", the V_d move to the same direction of final root, otherwise V_d goes to the opposite direction like the case in Fig. 15 (c). For the example in Fig. 16 (c), the value of the root is 0.1. With the initial value from about -13 to -10, the V_d goes to the opposite direction. Therefore, an infinite loop occurs, and it cannot reach the final value. By looking at the results in Fig (a)-(d), it can be seen the non-convergent condition happens when the sign of initial value is different from that of the root. However, the dynamic PV cell model simulates both forward and reverse biased regions, so the situation happens in many operating points. Although the computation performance of Halley's method is better than that of the NR method, but its reliability is low. Therefore, the Halley's method should not be used for dynamic PV cell model. The improved computation time methods are described in next chapter. The methods are applied to only the NR method because the Halley's method is not used in this paper.

4.2 Initial values for fast computation

The initial value is an important factor for convergence speed [5]. The closer the initial value is to the root, the shorter the calculation time. This paper describes three methods for selecting the initial value: the initial values of approximate PV cell equations, the initial values of the previous value of V_d, and the initial values of the combining method using the above two methods. The approximated PV cell equation is a simplification the full model of (2). In (2), there are four terms that depend on V_d, which are $I_{df}(T,V_d)$, $I_{dr}(T,V_d)$, $I_{Rsh}(G,V_d)$, and $I_{Cp}(V_d)$. If the terms $I_{dr}(T,V_d)$, $I_{Rsh}(G,V_d)$ and $I_{Cp}(V_d)$ are neglected in (2), only $I_{df}(T,V_d)$ will depend on V_d. By neglecting the terms, the equation (2) can be simplified so that an approximate V_d can be determined without using numerical iteration as follows:

$$0 = I_{ph}(\mathrm{G},\mathrm{T}) - I_{df}(\mathrm{T},V_d) - I_{pv} \tag{33}$$

$$0 = I_{ph} - I_s\left[\exp\left(\frac{V_d}{aV_t}\right) - 1\right] - I_{pv} \tag{34}$$

$$V_d = aV_t \times \ln\left(\frac{I_{ph} + I_s - I_{pv}}{I_s}\right) \tag{35}$$

where the voltage V_d in (35) is an approximated value and this approximated value can be used as an

effective initial value to find the exact V_d [5]. Conventionally, zero or the open circuit voltage has been used as the initial value for the PV cell model [5].

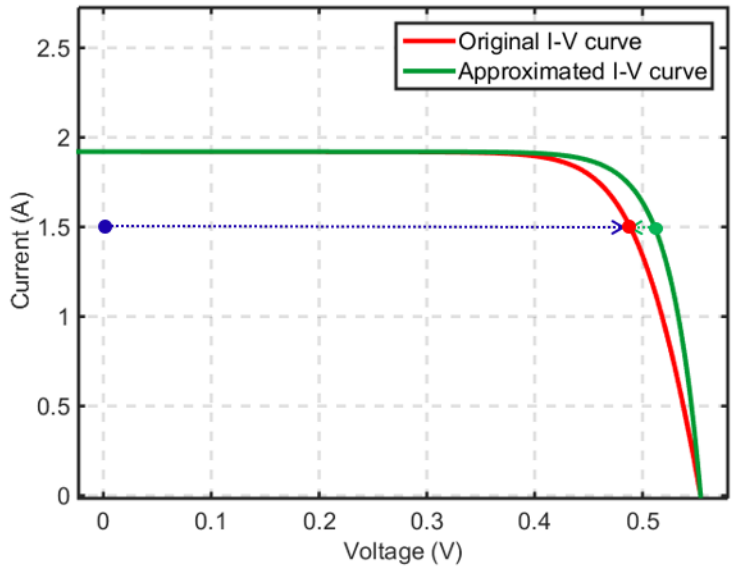

(a)

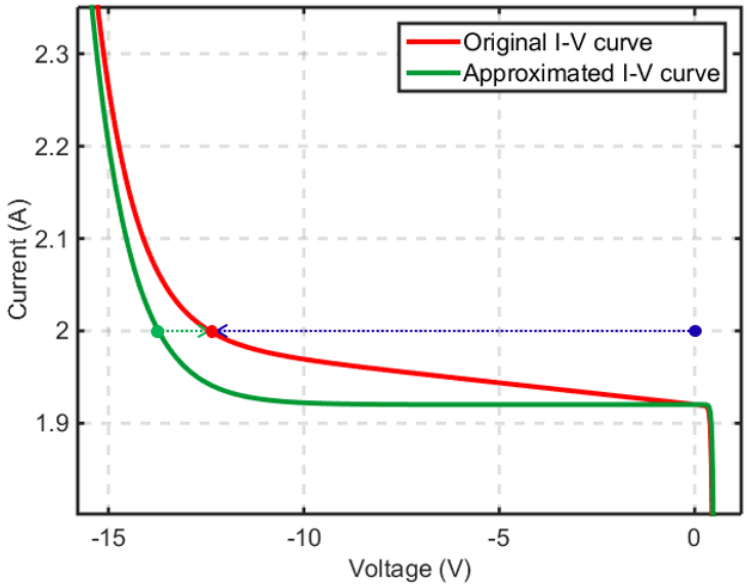

(b)

Fig. 17 Comparison of I-V curves: (a) Forward-bias region, (b) Reverse-bias region

Fig. 17 (a) shows the comparison of the original I-V curve and the approximated I-V curve in the forward-bias region. The I-V curves are close to each other, so the distance from the approximated initial value to the real value is shorter than that from zero to the real value. In the reverse-bias region, the effect of the forward diode is negligible, therefore the reverse diode should be used instead of the

forward diode. In the reverse-bias region, the approximated I-V curve can be obtained by replacing $I_{df}(T,V_d)$ with $I_{dr}(T,V_d)$ in (33). The approximated V_d can be expressed as follows:

$$V_d = aV_t \times \ln\left[\frac{-I_{pv}+\left(I_{scn}+K_i\right)\left(\frac{G}{G_n}\frac{M}{M_n}\right)+I_s}{I_s}\right], \quad \text{in the forward-bias region} \quad (36)$$

$$V_d = -\frac{aV_t}{K_r}\times \ln\left[\frac{I_{pv}-\left(I_{scn}+K_i\right)\left(\frac{G}{G_n}\frac{M}{M_n}\right)+I_{sr}\exp\left(\frac{K_rV_{bd}}{aV_t}\right)}{I_{sr}\exp\left(\frac{K_rV_{bd}}{aV_t}\right)}\right], \quad \text{in the reverse-bias region} \quad (37)$$

$$-I_{pv}+\left(I_{scn}+K_i\right)\left(\frac{G}{G_n}\frac{M}{M_n}\right) \quad (38)$$

where the values of I_s and $I_{sr}exp(\frac{K_rV_{bd}}{aV_t})$ are 1.07×10^{-9} and 3.34×10^{-8}, respectively, which are positive values and can be assumed as 0 for practical purposes. The sign of the equations inside the logarithm of (36) and (37) has to be positive and they are determined by (38). If (38) is positive, V_d in (36) is used as the initial value. In the other case, V_d in (37) is chosen as the initial value. With this approximated method, the effective initial value can be selected in both the forward and reverse biased regions.

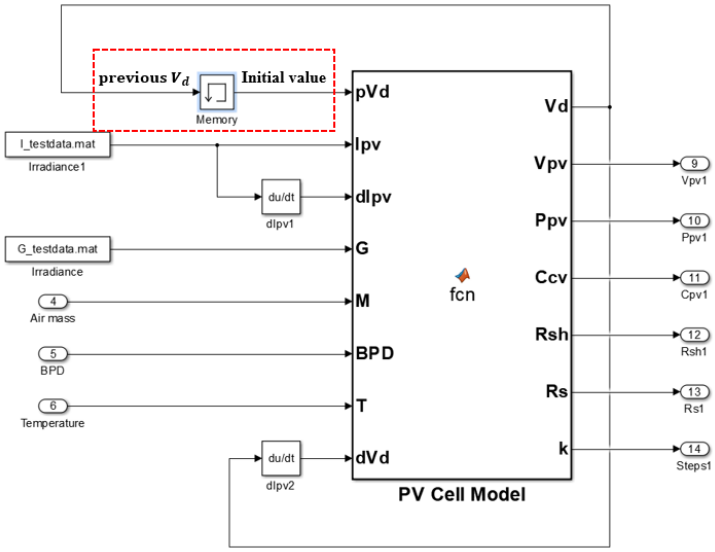

Fig. 18 PV cell model for the initial value from previous V_d

There is also another method to choose the initial value, which obtains an initial value from a previous solution. MATLAB/SIMULINK has a memory block that delays the input to the next

simulation time step. With this memory block, the previous value can be directly used as the next initial value shown in Fig. 18. The simulation time step is set to 50 μs in this model. The PV cell's output depends on environmental conditions such as irradiance and temperature. During the time step 50 μs, the environmental conditions do not hardly change so that the output change of the PV cell model is also small during the time step. Therefore, the previous value of V_d is similar to the current solution of V_d which is then determined using the numerical method. One of the model outputs is V_d and it goes into the memory block shown in Fig. 18. In the next step, the output value of the memory block is used for the initial value of V_d.

In most cases, the initial value from the previous solution is more effective than the approximated initial value. However, it is recommended to use approximated initial value when the PV cell's input suddenly changes in which the value of previous V_d is not similar to current value of V_d. Therefore, a method combining the approximated initial value and the previous value method is proposed. It selects the initial value according to the rate of change of the input variables. There are three dominant inputs of the PV cell: irradiance, cell temperature, and output current. Fig. 19 (a) shows the MATLAB/SIMULINK model using the proposed combined method. The function of the combined method has four inputs: value of the previous V_d, irradiance, cell temperature, and output current. If the change of the input values is small, the value of previous V_d is used as the initial value. In the opposite case, the approximated initial value is used. The reference value of the input change rate can be obtained by analyzing the PV cell model under various operating conditions. In this paper, the thresholds are set as $1.9\ W/\mathrm{m}^2 T_s$, $2.8\ K/T_s$, and $1\ mA/T_s$ for the irradiance, the cell temperature, and the output current, respectively. T_s is the simulation time step, which is 50 μs. Fig. 19 (b) shows the performance comparison of the approximated initial value and the previous value. The iteration number using the initial value of the previous V_d is less than that of the approximated initial value. However, the approximated initial value method shows fewer iterations in which the change rate of I_{pv} is higher than $1\ mA/T_s$. The lower iteration number means shorter computation time. The model computation time using each initial value is compared in Section IV.

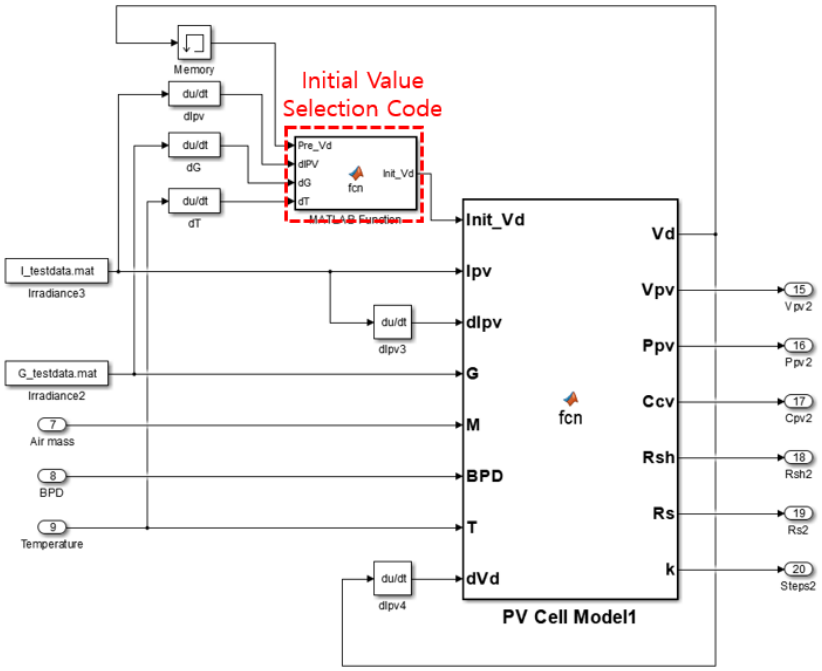

(a)

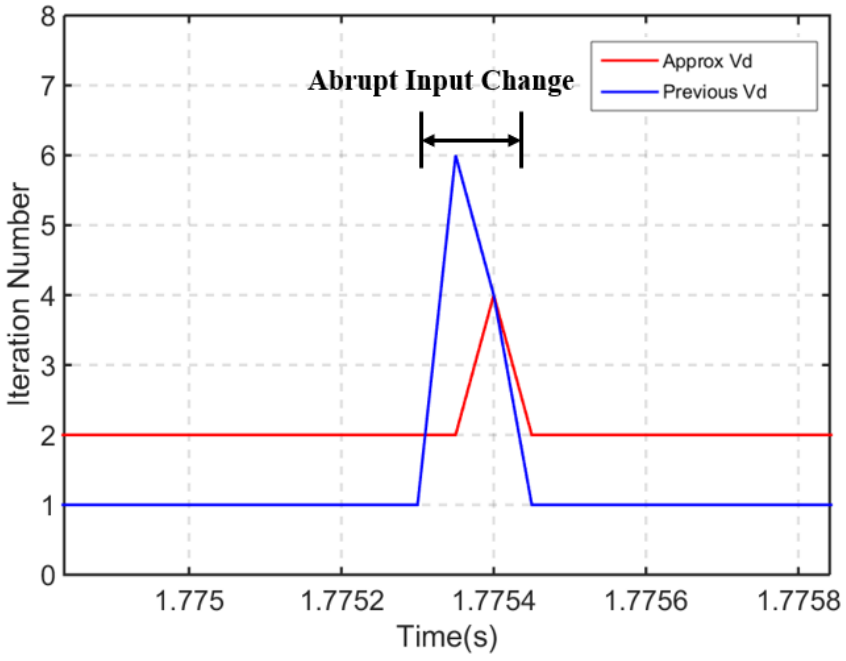

(b)

Fig. 19 Combined initial value method: (a) PV cell model, (b) Comparison of iteration number

V. PHILS and Experimental Results.

After applying the computation time improvement method, the accuracy of the PV cell model is verified. The PV cell model is verified under two operating conditions: in static and dynamic conditions. In the static condition, the accuracy of the PV cell model is verified in a PC-based non-real time simulation. In the dynamic condition, the accuracy of the PV PHILS system, which includes delays of a real-time simulation and a power interface, is verified. After the model is verified under two conditions, the computation time of the PV cell models, which use the conventional method and the three proposed methods, is compared.

5.1 Photovoltaic model verification

In the static condition verification, the I-V curve and the temperature of the PV cell are compared with the experimental data. Fig. 20 shows the result comparison of the I-V curve and the temperature according to irradiance conditions. In this paper, the error is calculated by the Mean Relative Error (MRE) method. The PV cell model accurately simulates actual PV cell model, and the MRE is measured as 1.43% in the I-V curve and 0.12% in the temperature, respectively.

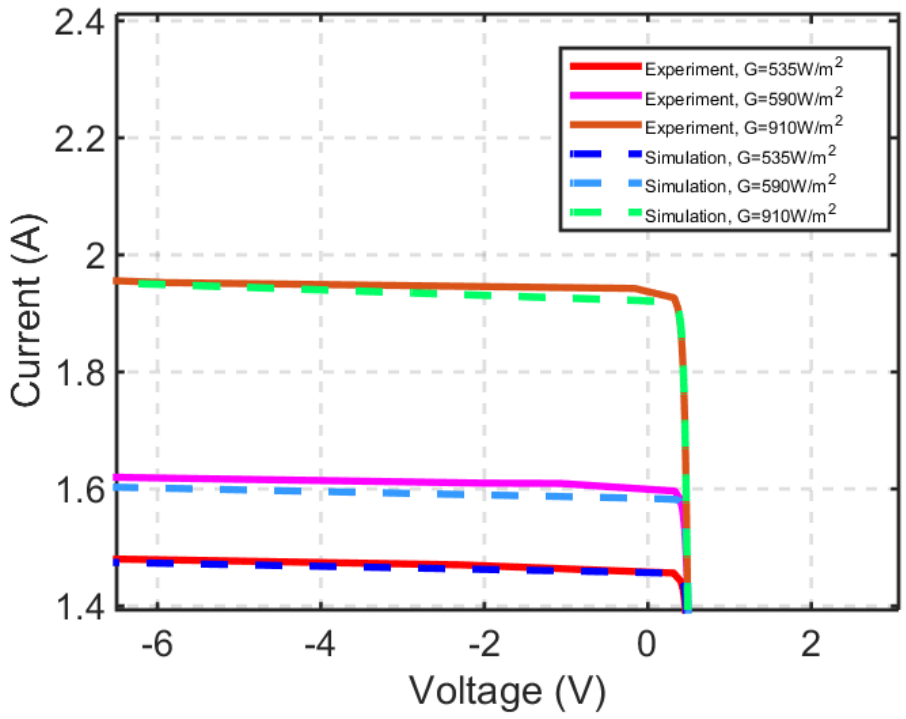

(a)

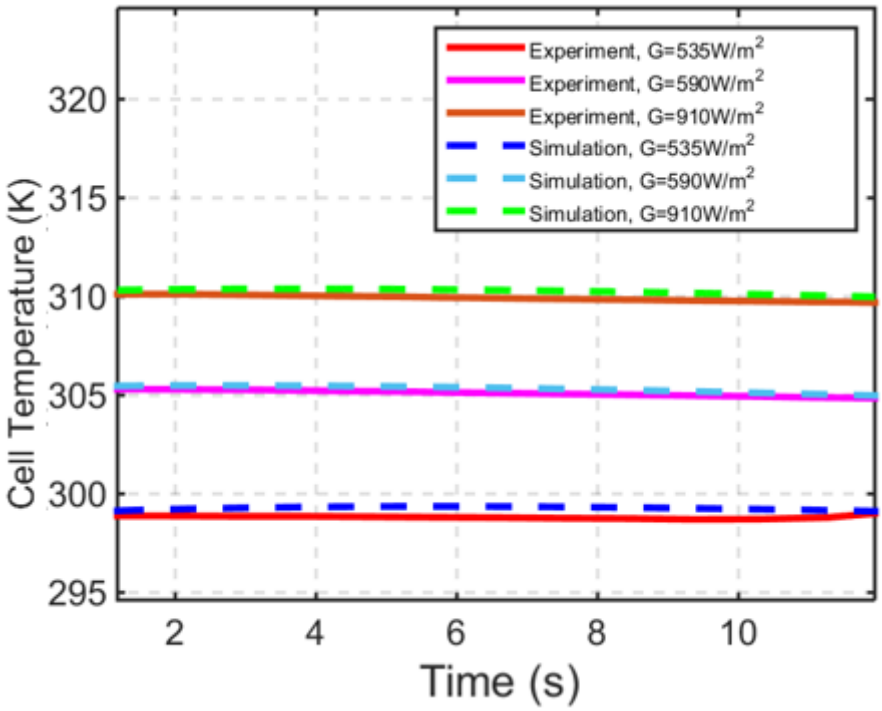

(b)

Fig. 20 Static verification results: (a) I-V curves and (b) Temperature curves.

In the dynamic condition, the input of PV cell suddenly changes to verify that PV PHILS system can simulate the dynamic characteristics of PV cell. The PV cell's output is the output voltage and one of most influential inputs is the output current, so the output voltage is observed according to sudden output current changes. Fig. 21 shows dynamic simulation results of the PV cell model. Fig. 21 (a) shows the input profile of the PHILS system. The output current is and controlled by the source meter. Fig. 21 (b) shows the output voltage of the PV PHILS and the experimental measurement according to the input profile. The MRE of the dynamic voltage is 1.18%. The time delay of the real-time simulator is 100 μs which is twice the simulation time step. In addition, the time delay of the programmable power supply is 150 μs. The total time delay of the PHILS system is around 250 μs, however, it is small enough to simulate the dynamic characteristics of PV cell [16].

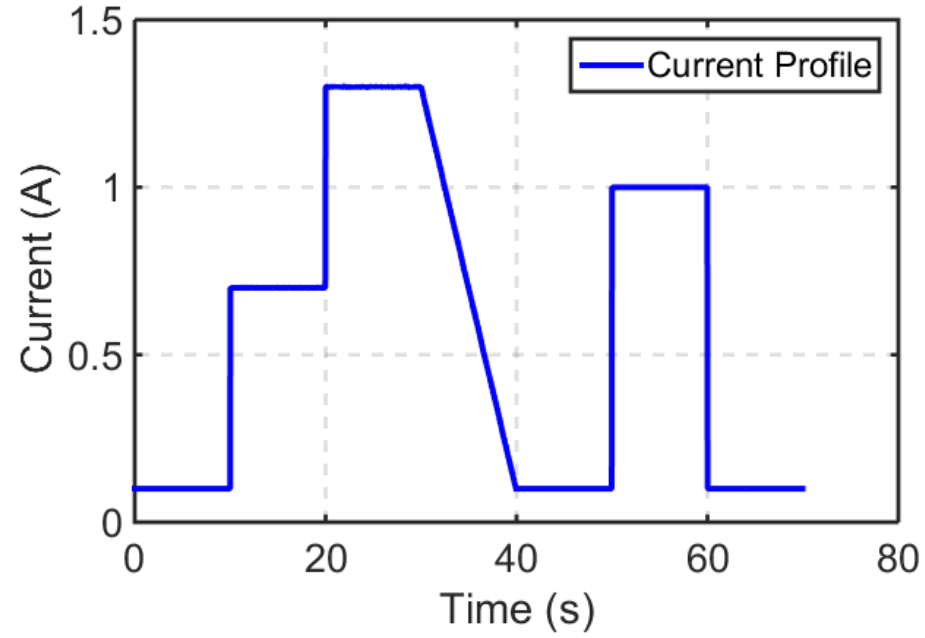

(a)

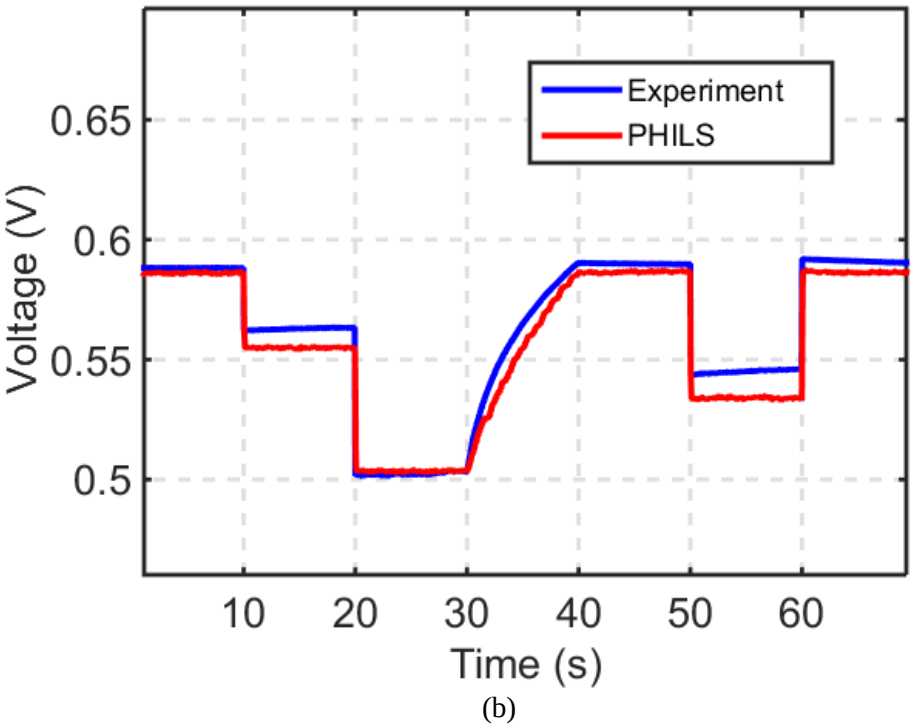

(b)

Fig. 21 Dynamic verification results: (a) Input profile, (b) Output voltage curves

5.2 Performance comparison results

In previous research, Halley's method was used for fast computation [3], [4], [14] and [15]. However, Halley's method cannot be used due to its inaccuracy for the electric-thermal dynamic PV

cell model. Therefore, the computation performance improvement by the initial values is shown only with the NR method. The PV model operates in static and dynamic conditions. In the static condition, the PV cell model operates under the irradiance range of 630~780 W/m^2.

Table II shows the model computation time of the conventional and proposed methods. Using the zero initial value, the computation time is 2.44 μs. With the approximated initial value, the computation time is reduced to 1.83 μs. By using the initial value from the previous V_d, the computation time is reduced to 1.66 μs. The results of the initial value from the previous V_d and the combined method is the same in the static condition. In this condition, the combined method uses only the initial value from the previous V_d because input variables do not change suddenly. In the dynamic condition, the sudden input changes occur, which result from abnormal operations such as partial shading and drastic output current changes in practical experiments. In this condition, the computation time is 3.49 μs, 1.93 μs, 1.71 μs and 1.67 μs for the zero, approximated V_d, previous V_d, and combined initial value, respectively. In this condition, the input change rates exceed the reference value. When the inputs suddenly change, the combined method uses the approximated initial value instead of the initial value from the previous V_d. By using the combined method, the fastest computation time can be obtained.

TABLE II COMPUTATION TIME OF PV CELL MODEL

Initial Value	Zero	Approximated V_d	Previous V_d	Combined Method
Computation Time (Static Condition)	2.44 μs	1.83 μs	1.66 μs	1.66 μs
Computation Time (Dynamic Condition)	3.49 μs	1.93 μs	1.71 μs	1.67 μs

VI. PHILS Application

Up to section 5, the operation and computation time is described for one PV cell model. In this section, the application of simple PV PHILS and the model extension are described. In the application of PV PHILS, the PV cell operates with a converter and, MPPT function test of the converter is performed. Also, PV PHILS system using DPP converter is simulated. In the model extension, the PV cell model is extended to the PV panel model and the maximum possible model number, which the real-time simulator can computes, are described according to the initial values.

6.1 MPPT operation of PV PHILS system

The implementation of the MPPT function is intended to show that PV PHILS simulates the practical operation of a PV cell. This allows verification of the dynamic performance of the PV PHILS system. The source meter operating as the power converter is controlled by the MPPT algorithm. The MPPT algorithm uses perturbation and observation (P & O) methods. This method continuously adjusts the output current to a small step size (0.02 A) in the direction of increasing power. Due to the nature of this algorithm, the MPP is never achieved exactly. However, the operating point get close to the MPP and PV cell operates near MPP. The MPPT sampling time is chosen to be 30 ms, which is sufficient for normal operating conditions [17], [18].

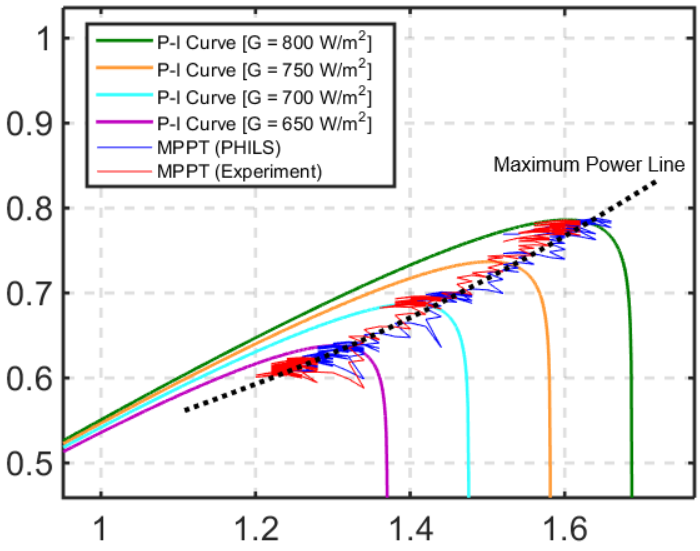

Fig. 22 MPPT operation result

Fig. 22 shows the power trajectory of the PV cell near the four power-current curves at 800, 750, 700, and 650 W/m^2 irradiance respectively. The operating point starts at I_{pv} = 1.52 A. The operating point oscillates around the MPP by the MPPT algorithm. The dynamic performance of the

proposed PHILS system is close to that of the experimental measurements and operates within an MRE of 2.2%. This value is sufficient for the target PV PHILS applications. In conclusion, the emulated PV cell by the proposed PHILS technique can accurately calculate the practical PV cell's operating characteristics in static and dynamic conditions.

6.2 Performance improvements in large-scaled PV panel model.

The computation time reduction for the single cell looks not significant according to the simulation time step (50 μs). In order to show the computation speed enhancement of the large-scaled PHILS system in practical manner, the PV cell model can be extended to the PV panel model. It is more practical because all the power generations from the PV system are based on the series and parallel connections of the PV panels.

The operational conditions of the PV panel model are referred to the PV panel experiments conducted by the previous research [19]. In the previous research, a 140 W polycrystalline PV panel is used, and the PV panel model using the proposed method is verified using the I-V curve of the actual PV panel, which is shown in Fig. 23 (a). The I-V curves are measured under the partial shaded condition of the single PV panel shown in Fig. 23 (b). The PV panel model is divided into two parts which have different irradiance inputs for normal and partial-shaded cases of 926 and 193 W/m^2, respectively. The I-V curve verifies the accuracy of the PV panel model used in this paper.

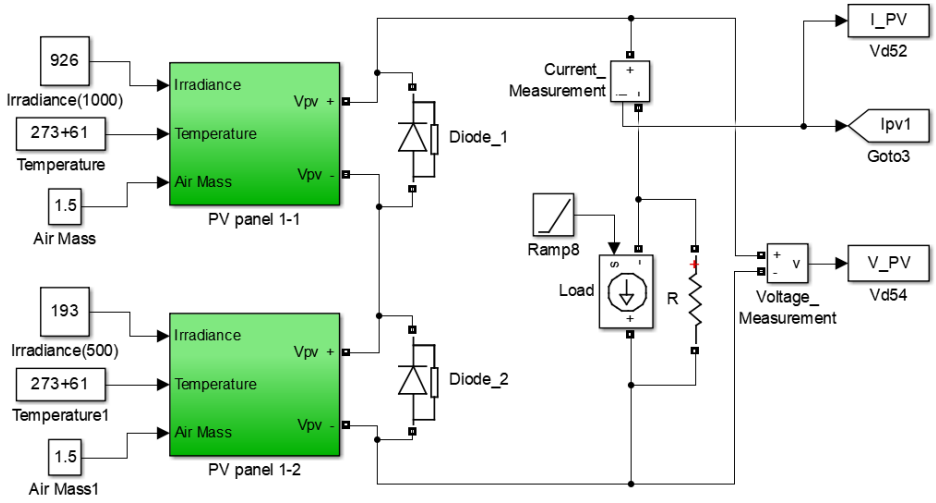

(a)

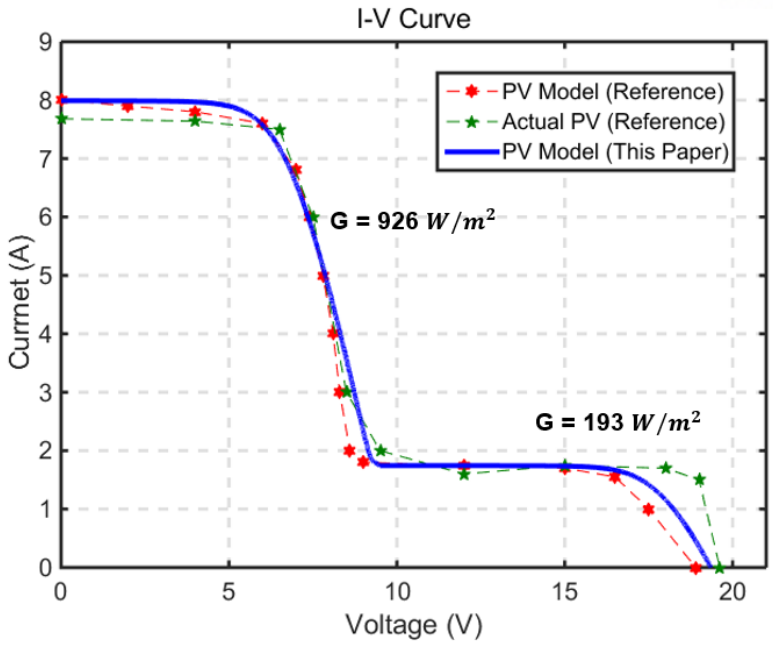

(b)

Fig. 23 Modeling of PV Panel: (a) PV panel model, (b) PV I-V curve

Table III shows the computation time of the PV panel model according to the initial values. The computation speeds are compared according to the estimating methods of the initial value under steady-state and transient condition. The proposed method shows better computation performance than the conventional method which uses the initial value as zero. The combined method shows the fastest computation speed even in the panel model. The computation time of previous V_d shows faster than that of approximated V_d as verified in section III-B. In transient condition, combined method shows better performance than previous V_d because, the combined method uses the approximated V_d when the sudden input change occurs.

In order to show the computation performance of the combined method in another aspect, the other simulation result is described. The real-time simulator can also simulate multiple panels within simulation time step, which is set to 500 us for the PV panel simulation. If the simulation computation time exceeds the time step, overrun error occurs which reduces the accuracy of the PV panel model. Therefore, the simulation computation time should not exceed the time step. The maximum number of PV panel models, which the real-time simulator calculates within the time step, is different according to initial value methods. Fig. 24 shows the comparison of the computation time and the maximum numbers of PV panels for the conventional method and the combined method. The shape of the computation time graph looks like a pulse wave because the PV panel models are simulated in the transient condition where the sudden input changes happen periodically. In Fig. 24, it is observed that the form of computation time of two methods is different. The difference between the maximum

computation time and the minimum computation time is large with the combined method. This is because the combined method has high computation performance in steady-state condition described in section III-B. The real-time simulator can compute 6 PV panel models for the conventional method and 32 models for the combined method. The computation time is reduced by 86.7% and the maximum number of PV panel models, which real-time simulator can compute, increases about 5 times with the proposed computation time improvement method.

TABLE III COMPUTATION TIME OF PV PANEL MODEL

Initial Value	Zero	Approximated V_d	Previous V_d	Combined Method
Computation Time (Steady-state Condition)	29.35 μs	6.22 μs	4.52 μs	4.52 μs
Computation Time (Transient Condition)	38.91 μs	9.85 μs	5.29 μs	5.19 μs

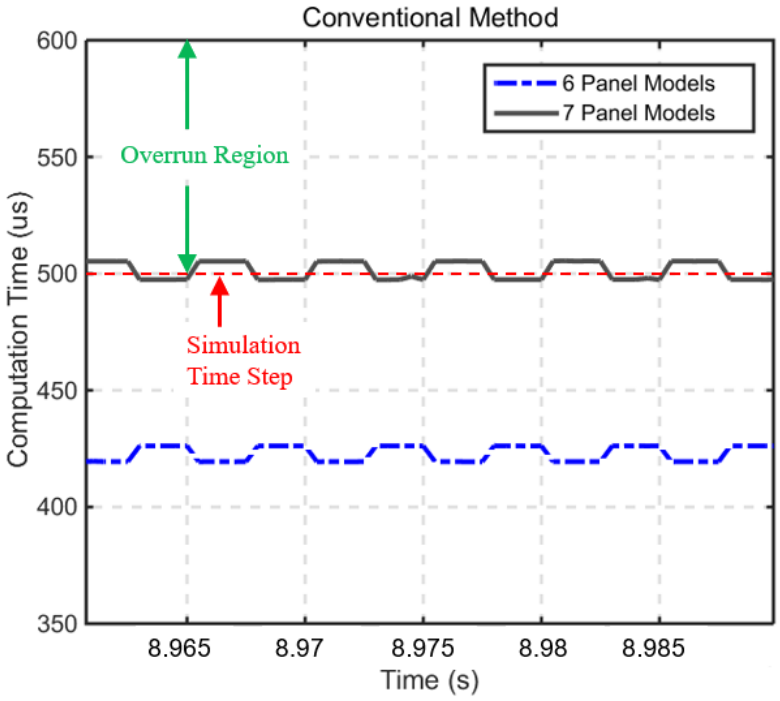

(a)

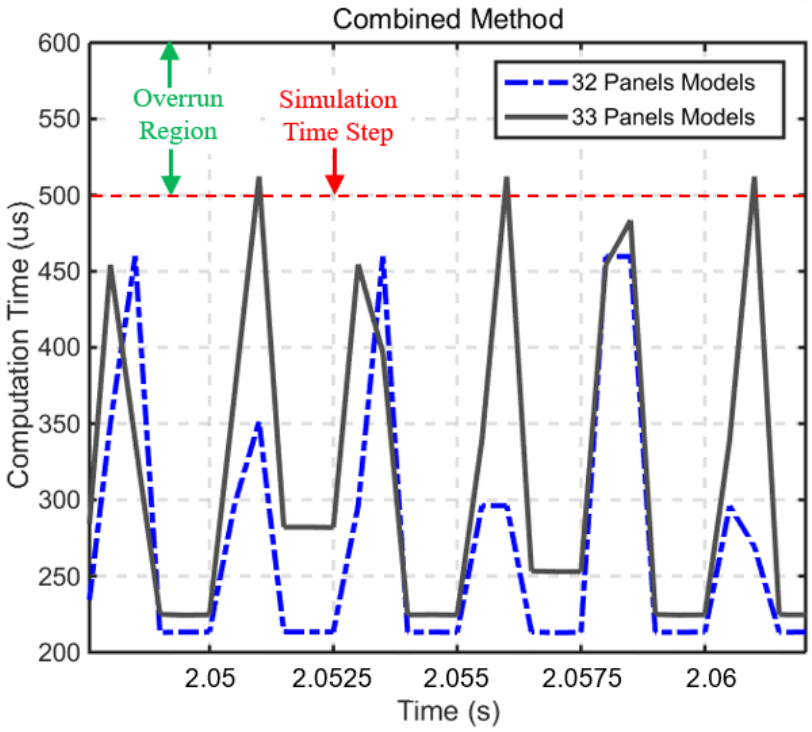

(b)

Fig. 24 Computation time of PV panel model: (a) Conventional Method, (b) Proposed Method

6.3 Simulation of DPP converter operation

PHILS is a platform allowing to simulate a virtual system and test the operation of the prototype. In order to save the time of the operation test, the PHILS system should be prepared in advance to test the prototype as soon as it is developed. Therefore, the PHILS system should be prepared with the development of the prototype. This section describes the PHILS system for the PV system using the DPP converter to be developed. The DPP converter operates in parallel with the PV panel and performs the MPPT operation with high efficiency in the partial shading condition [20]. Fig. 25 shows a conceptual diagram for the PV PHILS system.

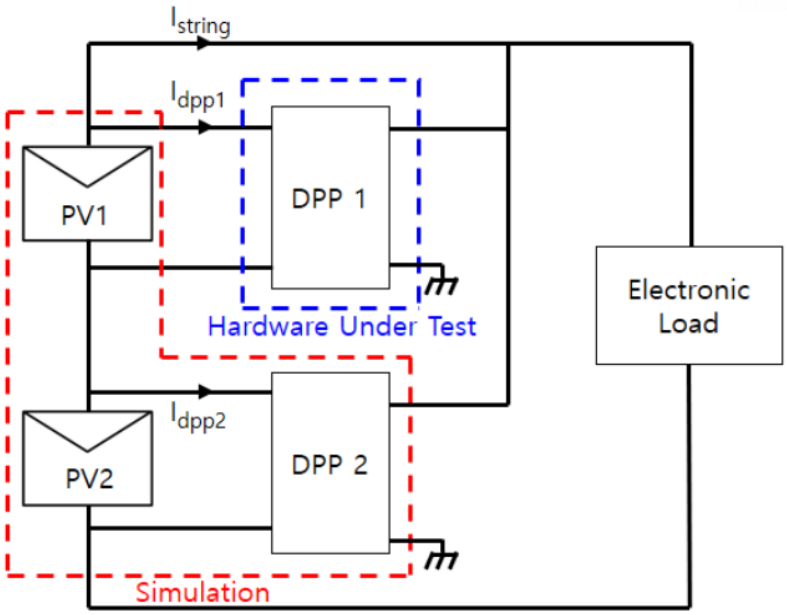

Fig. 25 Conceptual diagram of the PV PHILS system

The same two DPP converters would be operated in the PHILS system, one DPP converter would operate as a simulation model, and the other DPP converter would be tested as an actual hardware. However, the PHILS platform is currently being prepared without a DPP converter prototype being developed. Therefore, both the DPP converters are simulated with the current source model and the MPPT algorithm so that only simple operation can be implemented shown in Fig. 26. Fig. 27 (a) represents the output power of each PV cell in the partial shading situation, which is controlled by the DPP converter with the MPPT algorithm. Fig. 27 (b) represents the output voltage of the DPP converter. The PV panel model operates well with the control of the DPP converter, and the voltage of the DPP converter is well simulated through the power interface device. When DPP converter is developed, DPP converter 1 will be tested with real hardware and DPP converter 2 will be modeled with real DPP converter to construct PHILS system.

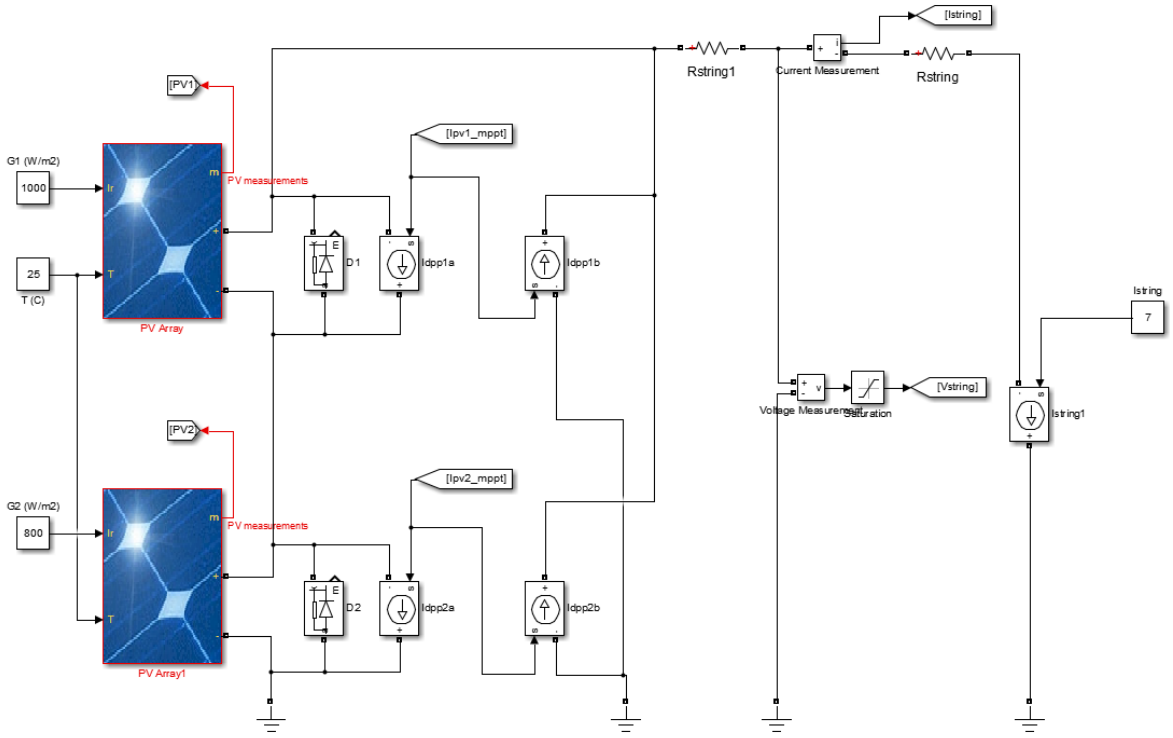

Fig. 26 DPP converter PV system model

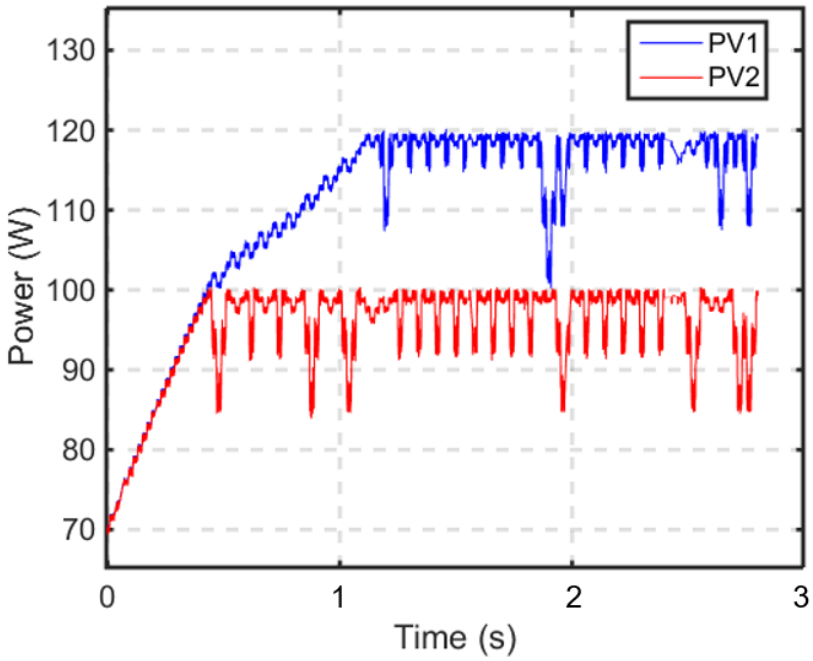

(a)

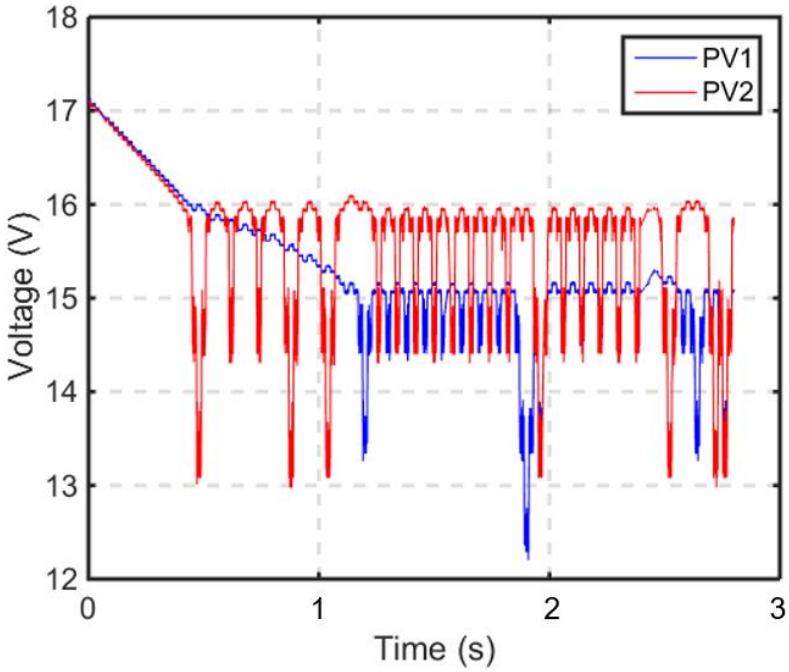

(b)

Fig. 27 PHILS results (a) PV panel power (b) PV panel voltage

VII. Conclusions

In this paper, efficient methods of solving the numerical solution have been proposed. First, the determining method whether a numerical solution is appropriate is described by applying Newton-Raphson and Halley's method to the PV cell model. Halley's method could not be used in the dynamic PV cell model because it did not converge in some regions. Secondly, efficient initial value selection methods have been described. These methods considerably reduce the calculation time of the PV cell model. The computation time is reduced by 52.15% compared to the conventional method by applying the fastest method among the proposed methods to verify the accuracy of the proposed method, the PV cell model is compared with the actual PV cell operation results under static and dynamic operating conditions and the model error is within 1.43%. In addition, two PHILS applications are described to describe the development of a power converter using PHILS. The MPPT function test of a power converter show the PHILS system can simulate the dynamic characteristics of the PV cell. The real-time simulation for the PV panel show the real-time simulator can simulate 5 times larger model than before with the proposed initial value selecting method. The simulation of DPP converter operation shows how to prepare PHILS system.

.

VIII. Future Plan

1. PHILS setup for DPP converter function test.

The control method of the photovoltaic system using the DPP converter has a more complicated structure than the existing system. Therefore, the PHILS test platform can be used efficiently to perform the operation test of the DPP converter, which can help fast development. PHILS must be able to operate in conjunction with HUT at the same time as development. Therefore, the model should be prepared before the product is developed. Now, the simple source model simulates DPP converter. In the future, the system will be constructed by modeling the actual DPP converter. When the actual hardware of the DPP converter is developed, the PHILS test will be performed based on the PV system model composed of several PV cells and DPP converters.

2. HILS for ship Power Management System (PMS)

The PMS is a device that controls the power system to operate efficiently and stably. PMS is also used on ships to control the ship's power system. If the PMS malfunctions, it can cause a big accident due to unknown reasons and it can result in ship development. Therefore, the operation of the PMS should be tested under various conditions before being applied to the ship. In order to perform PMS operation test through HIL, a model simulating the ship's power system in real-time should be constructed Therefore, I would research on development of a model that can simulate the ship power system in real time based on the diagram of the ship power system and reliability verification of the model.

REFERENCES

1. H.-R. S, M. Park, I.-K. Yu, B.-M. Song, "Performance analysis and evaluation of a multifunctional grid connected PV system using power hardware-in-the-loop simulation," in *Proc. IEEE Applied Power Electronic Conference and Exposition (APEC)*, 2011, pp. 1945-1948.

2. D. S. Karanjkar, S. Chatterji, S. S. L., A. Kumar, "Real time simulation and analysis of maximum power point tracking (mppt) techniques for solar photo-voltaic system," in *Proc. Recent Advances in Engineering and Computational Sciences*, 2014, pp. 1–6.

3. J.-H. Jung, S. Ahmed, "Real-time simulation model development of single crystalline photovoltaic panels using fast computation methods," *Solar Energy*, vol. 86, no. 6, pp. 1826-1837, Jun. 2012.

4. J.-H. Jung, "Power hardware-in-the-loop simulation (PHILS) of photovoltaic power generation using real-time simulation techniques and power interfaces," *Journal of Power Sources*, vol. 285, pp. 137-145, 2015.

5. H. Can, D. Ickilli, and K. Parlak, "A new numerical solution approach for the real-time modeling of photovoltaic panels," in *Proc. Asia-Pacific Power and Energy Engineering Conference (APPEEC)*, 2012, pp. 1–4.

6. M. G. Villalva, J. R. Gazoli, and E. Filho, "Comprehensive approach to modeling and simulation of photovoltaic arrays," *IEEE Trans. Power Electron*., vol. 24, no. 5, pp. 1198–1208, May. 2009.

7. Y. Mahmoud, W. Xiao, and H. H. Zeineldin, "A parameterization approach for enhancing PV model accuracy," *IEEE Trans. Ind. Electron*., vol. 60, no. 12, pp. 5709–5716, Dec. 2013.

8. A. Sarwar, M. Hasan, and A. Ansari, "Five parameter modelling and simulation of solar PV cell," in *Proc. International Conference on Energy Economics and Environment (ICEEE)*, 2015, pp. 1–5.

9. K. A. Kim, P. T. Krein, "Photovoltaic hot spot analysis for cells with various reverse-bias characteristics through electrical and thermal simulation," in *Proc. IEEE Workshop Control Modeling Power Electron*., 2013, pp. 1–8.

10. K. A. Kim, C. Xu, J. Lei, P. T. Krein, "Dynamic photovoltaic model incorporating capacitive and reverse-bias characteristics," *IEEE J. Photovoltaics*, vol. 3, no. 14, pp. 1334-1341, Oct. 2013.

11. A. Jones, C. Underwood, "A thermal model for photovoltaic systems," *Solar Energy*, vol. 70, no. 4, pp. 349-359, Feb. 2001.

12. X. H. Mai, S-K Kwak, J-H Jung and K. A. Kim, "Comprehensive Electric-Thermal Photovoltaic Modeling for Power Hardware-in-the-Loop Simulation (PHILS) Applications," *IEEE Trans. Ind. Electron*., vol. 64, no. 8, pp. 6255-6264, Mar. 2017.
13. S. Chapra, *Applied Numerical Methods with MATLAB for Engineers and Scientists 3/e.* New York: McGraw-Hill, 2012, pp. 158-160.

14. G. Alefeld, "On the convergence of Halley's method," *American Mathematical Mo nthly*, vol. 88, pp. 530-536, 1981.

15. A. Melman, "Geometry and convergence of Euler's and Halley's methods", *SIAM review*, vol. 39, no. 4, pp. 728-735, Dec. 1997.

16. R. J. Serna, B. J. Pierquet, J. Santiago, and R. C. N. Pilawa-Podgurski, "Field measurements of transient effects in photovoltaic panels and its importance in the design of maximum power point trackers," in *Proc. IEEE Applied Power Electronics Conf. and Exposition*, 2013, pp. 3005– 3010.

17. M. Andresen, G. Buticchi, and M. Liserre, "Thermal stress analysis and MPPT optimization of photovoltaic systems," *IEEE Trans. Ind. Electron*., vol. 63, no. 8, pp. 4889–4898, Aug. 2016.

18. F. M. Oliveira, S. A. O. Silva, F. R. Durand, L. P. Sampaio, V. D. Bacon, and L. B. G. Campanhol, "Grid-tied photovoltaic system based on PSO MPPT technique with active power line conditioning," *IET Power Electron.*, vol. 9, no. 6, pp. 1180–1191, Apr. 2016.

19. B. A. Alsayid, S. Y. Alsadi, J. S. Jallad, and M. H. Dradi, "Partial Shading of PV System Simulation with Experimental Results," Smart Grid Renew. Energy, vol. 04, no. 06, pp. 429–435, 2013.

20. P. S. Shenoy, K. A. Kim, P. T. Krein, and P. L. Chapman, "Differential power processing for efficiency and performance leaps in utility-scale photovolatics," in Proc. IEEE Photovoltaics Spec. Conf., 2012.